The University of Alberta
Printing Department
Edmonton, Alberta

THE UNIVERSITY OF ALBERTA

AN INVESTIGATION OF THE USE OF THE STRESS INTENSITY FACTOR FOR FATIGUE CRACK PROPAGATION STUDY USING A SINGLE-EDGE-NOTCH SPECIMEN

by

© ARTHUR MICHAEL DANIELSON

A THESIS

SUBMITTED TO THE FACULTY OF GRADUATE STUDIES

IN PARTIAL FULFILMENT OF THE REQUIREMENTS FOR THE DEGREE

OF MASTER OF SCIENCE

DEPARTMENT OF MECHANICAL ENGINEERING

EDMONTON, ALBERTA

JUNE, 1968

UNIVERSITY OF ALBERTA

FACULTY OF GRADUATE STUDIES

The undersigned certify that they have read, and recommend to the Faculty of Graduate Studies for acceptance, a thesis entitled "An Investigation of the Use of the Stress Intensity Factor For Fatigue Crack Propagation Study Using a Single-Edge-Notch Specimen" submitted by ARTHUR MICHAEL DANIELSON in partial fulfilment of the requirements for the degree of Master of Science.

ABSTRACT

The stress intensity factor K, a parameter used in Fracture Mechanics, is applied to the study of the crack propagation stage of fatigue.

It was necessary to find K for a single-edge-notch specimen using a fatigue crack for the notch. Long single wire strain gauges were used to measure the SEN specimen compliance from which K was calculated. Corrections for plastic zone at the crack tip were applied to crack length. The expressions and values for K were found to be in good agreement with those that had been published for use in fracture toughness tests.

The crack propagation rate da/dN, is correlated with K using a K versus log (da/dN) plot and a log (K) versus log (da/dN) plot. These correlations were affected by the stress ratio, and the specimen thickness. A comparison is made with published correlations and the differences are discussed. Fatigue cracks are discussed in relation to the experimental method required to measure the crack length, the slanting of the fatigue surfaces, the validity of K for fatigue cracks, and published observations of electron fractography of the fatigue crack surfaces.

ACKNOWLEDGEMENTS

This thesis was prepared under the supervision of Dr. G. Ford.

The writer is indebted to Mr. J.A. Dunsby of the National Aeronautical Establishment for introducing the problem investigated; to Ray Marak and Andy Smart for aiding in the experimental apparatus; and to the National Research Council for financial support.

TABLE OF CONTENTS

CHAPTER PAGE

LIST OF TABLES

LIST OF FIGURES

FIGURE PAGE

NOTATION

a	Crack length
a_c	Crack length corrected for plastic effects to an equivalent elastic crack length
C	Compliance $(\frac{e}{p})$
e	Displacement of loading points
E	Modulus of elasticity in tension
G	Strain energy release rate due to a unit length of crack growth in a sheet specimen of unit thickness, also called the crack extension force
G_c	Fracture toughness - the critical value of the strain energy release rate at which the crack length becomes unstable
K	Stress intensity factor
ΔK	Stress intensity factor based on the stress range
P	Load per unit thickness of specimen
R	Ratio of minimum to maximum cycling stress called stress ratio
r, θ	Curvilinear coordinates for the area around the crack tip
r_y	Radius of plastic zone approximation
S	Energy gain of a specimen due to the creation of a new surface
SEN	Single-Edge-Notch
T	Surface tension of a material

U	Increase in potential energy plus the increase in strain energy due to the crack. Includes energy changes due to surface tension, plasticity, etc.
u, v	Displacement in x, y directions
V	Strain energy
V_o	Initial potential energy for a body with a crack length of zero length
w	SEN specimen width
W	Increase in strain energy due to the crack
x, y	Rectangular coordinates for the area around the crack tip
μ	Poisson's ratio
σ	Stress
σ_{ys}	Yield stress

CHAPTER I

INTRODUCTION

1.1 A Fracture Mechanics Approach to Fatigue

Fatigue, which may be considered fracture under cyclic loading, has been one of the most common causes of service failures. Fatigue cracks form fairly early in the life of materials after which they propagate in an assumed continuous process.

The study of the crack propagation stage of fatigue can be aided by certain parameters of Fracture Mechanics. These parameters are the stress intensity factor, which is used in describing the stress field around the crack tip, and the strain energy release rate which is used in describing energy changes of a specimen with a propagating crack. Application of these parameters to fatigue crack propagation is discussed with respect to corrections and the use of the single-edge-notch (SEN) specimen.

The SEN specimen has recently been developed for studying fracture under "static" loadings. Expressions of the stress intensity factor were developed for these fracture tests. Studies on fatigue crack propagation have used the SEN specimen with the expressions of the stress intensity factors which were developed for the crack under plane strain conditions. Experimental determination of the stress intensity factor for the SEN specimen using a fatigue crack for the notch, was thought useful in checking the values of the stress intensity factor of the fracture test. The dependence

of the crack propagation rate on the stress intensity factor is investigated.

1.2 Historical Review

In the past century, advances in transportation, automatic production equipment, and prime movers have created a situation where fatigue failures have become common. To prevent fatigue failures, the performance of materials subjected to cyclic loads and stress concentrations have been investigated since the mid 1800's.

In 1870, Wohler published the results of his twenty year study on fatigue failures. His work resulted in the S-N curve which has become one of the factors in evaluating the performance of engineering materials subject to cyclic loads. The use of the S-N curve was the basis for the first scientific design of structures subjected to repeated stresses. This is one of many approaches that have been used to describe the basic mechanism and controlling factors of fatigue, but none have been applied satisfactorily to structural design.

Gohn [1] and Hardrath [2] have reviewed various fatigue theories. Gohn states that

> up to a certain stage in development each of the theories is in accord with the observed phenomena, but to complete the theory certain assumptions are usually made upon which no experimental evidence is available. The theory, therefore, can not be proved, but neither can it be disproved.[1]

---

1 Gohn, Fatigue of Metals, 1963, pp. 107.

Considering the crack propagation stage of fatigue, Paris and Erdogan [18] proposed the theory that the crack propagation should be a function of the stress intensity factor. They showed that their theory agreed with a wide range of data; better than the other theories on crack propagation.

The development of the concept of "Fracture Mechanics" started in 1920, with Griffith's [3] concept of unstable crack propagation. He considered the crack length would become unstable if the total energy of the system was lowered for an increase in crack length. Essentially, he considered a balance between the strain energy of the system and the crack surface energy. He could then predict the conditions under which a flaw of given size in the system, would increase in size, usually resulting in complete failure. Due to evidence of plastic deformation on fractured surfaces, the energy needed for plastic deformation was added to the surface energy term [4].

In 1954, Irwin and Kies [5] developed expressions for the strain energy release rate in terms of specimen compliance changes due to crack growth. Later, in 1957, Irwin [6] made a theoretical analysis of the stress and strain near the end of a sharp crack, with the stress intensity factor being the governing parameter of the stress strain equations. The stress intensity factor, K, takes care of the influence of the configurations, loads, and changing crack length of the specimen for the stress strain expressions. Irwin [6] related K to the strain energy release rate, G. The stress analysis of several specimens were given, from which K was calculated.

For specimens of an arbitrary design, alternative methods will yield sufficiently accurate K expressions. These are:

(1) Theoretical stress analysis procedures [13, 14]

(2) Experimental strain analysis procedures using photoelasticity and strain gauges [6]

(3) Experimental measurements of specimen compliance as a function of crack length [5].

Since World War II the extensive investigations of many fractures has led to most of the development and application of Fracture Mechanics to the problems associated with fatigue crack propagation. R.E. Peterson [7], in reviewing design aspects required in preventing fatigue failures, cites the widely known fatigue failures of the Comet I aircraft as a major incentive in the aircraft industry to investigate fatigue and design to prevent such failures in larger modern aircraft. Consequently, most of the recent work in fatigue crack propagation has been done by research facilities affiliated with the aircraft industry.

In the early nineteen fifties, a steel with a yield strength above 200,000 psi had been developed and was selected for use in a Polaris Motor Case [8]. Some of these missiles unexpectedly blew up in the air, others burst in hydrostatic tests and some even fractured in manufacturing due to the brittle nature of the high strength steel. As a result, in 1958 the special ASTM Committee on Fracture Testing of High-Strength Sheet Material was set up to provide a focal point of interest, talent, and information in the

field of fracture. The wide acceptance and use of K and G was partly due to the five reports of the committee.

The understanding of the strength and fracture of materials has increased tremendously in the past decade both from the macroscopic (fracture mechanics) viewpoint and the microscopic viewpoint. Conferences, such as the International Conference of Fracture [9] held in Sendai, Japan in September 12-17, 1965 which presented both the macroscopic and microscopic viewpoint tended to promote more complete understanding of fractures. The concepts of fracture of solids has advanced to the point where they can be used by practising engineers.

With the fairly recent development of the fracture parameters K and G, many test methods and specimens have been used to measure K and G for various materials. The SEN specimen has been one of the more recent specimens developed to enable testing with smaller machines and less equipment.

1.3 History of the Single-Edge-Notch (SEN) Specimen

The SEN specimen was initially introduced by Sullivan [11] as a new specimen design for plane strain fracture toughness tests. It has definite advantages over the center notch and double edge notch sheet specimens that were currently being used. Less material, smaller loading capacity of the test machines are required, and only one crack tip is observed in comparison with two crack tips of other specimens. The SEN specimen is a metal sheet, containing a crack (notch) at the edge midway between the supports, which

propagates from one edge of the sheet to the other; due to a pin loading applied at the ends of the long specimen. The continuously changing configuration and stress distribution of the SEN specimen, brought about by the growing crack, are accounted for by the stress intensity factor.

Sullivan [11] employed experimental compliance measurements to obtain expressions for K. The small size of the test specimen and certain features of her test procedure caused Srawley, Jones, and Gross [15] to question the accuracy of the K values. They found more accurate values of K using larger, longer specimens together with more accurate experimental techniques. In order to check the accuracy of these values, Gross, Srawley, and Brown [13] applied boundary collocation procedures to a suitable stress function, to obtain a K expression for the SEN specimen. Srawley, Jones, and Gross [15] found their K expressions to be in excellent agreement with those found by Gross, Srawley, and Brown [13], and disagreeing with the K expressions of Sullivan's [11].

The K expressions of references 13 and 15 were for a sharp crack in a perfectly elastic material in a plane strain state. However an actual crack has a plastic zone at the crack tip for which a correction must be made.

The SEN specimen is now commonly being used in fatigue crack propagation studies. In this investigation it was thought useful to obtain K values using a SEN specimen with an actual fatigue crack for the notch, rather than an artificial crack as used by Srawley et al.

CHAPTER II

THEORY

2.1 Griffith's Work

Griffith [3] proposed a crack propagation theory in 1920 that was the ground work of the present fracture mechanics energy concepts. He investigated the effects of surface treatments on the strength of metallic machine parts. Griffith found that small scratchs reduced the strength of parts and that the hypothesis of rupture of the present day did not account for this effect.

In considering a theoretical criteria of rupture he adopted the Theorem of Minimum Potential Energy, and applied it to an elliptic shaped flaw in a plate. His statement of the criterion is,

> if a system can pass from the unbroken to the broken condition it must do so by a process involving a continuous decrease in potential energy.[2]

If the potential energy of a specimen containing a crack is differentiated with respect to the crack length, and if the differential is positive, there is an increase in potential energy for an increase in crack length. The crack is therefore stable. If on the other-hand the differential is negative, the potential energy would decrease for an increase in crack length and hence the crack is unstable and will increase in length until the potential energy has reached a minimum value.

---

2 Griffith, Ruptures and Flow in Solid, Philosophical Transaction, Vol. 221, p. 165.

Griffith considered the changes in the potential energy for a specimen with a crack to be made up of the increase in strain energy W, and the surface energy S. To illustrate Griffith's concept, consider an example from Weiss and Yukawa [4] where an elastic crack of length 2a in an infinite plate of unit thickness is considered. A uniaxial stress σ is applied at infinity, perpendicular to the crack. The total change of strain energy due to the crack is

$$W = \frac{-\sigma^2 \pi a^2}{E}$$

The energy gain of the plate due to the creation of the new surface having a surface tension T, is

$$S = 4aT$$

The total decrease of potential energy is W plus S. If the crack length is taken as the only variable, the conditions for equilibrium and stability are found by differentiating the potential energy with respect to the crack length. Let the initial value of potential energy for zero crack length equal V_o.

The differential is

$$\frac{d}{da}(W + S + V_o) \qquad (1)$$

If then $\frac{d}{da}(W + S + V_o) < 0$ (1a) The crack length is stable

$= 0$ (1b) The crack length is critical

> 0 (1c) The crack length is unstable

Substituting the values of W and S in equation (1b) yields

$$\sigma = \left(\frac{2ET}{\pi a}\right)^{1/2}$$

as the value of stress at which the crack length is on the verge of increasing in length and is considered the critical crack length.

Experimental work of the nineteen forties showed plastic deformation to be evident on fracture surfaces. Orowan concluded that the changes in potential energy due to crack growth must include the work done in plastic deformation [4]. The absolute change in the strain energy must equal the absolute changes in surface energy plus the plastic work. The change in strain energy for an increment in crack growth for a unit thickness, is known as the strain energy release rate G. The strain energy release rate can be calculated by theoretical or experimental analysis. The other parts that make up the changes in strain energy are unknown. Values of G, found experimentally, can be used to predict the conditions for which a crack length will become unstable. These are known as the critical values of G or the fracture toughness G_c. For the example considered previously, the expression for the energy release rate is:

$$G = \frac{\pi a \sigma^2}{E} \qquad (2)$$

In the following sections, G is related to the stress strain field around a crack tip and to experimentally measurable values of the compliance of specimens. These relationships are used for the SEN specimen under consideration.

2.2 Stress Strain Field Around the Crack Tip

Irwin [6] obtained expressions for the stress strain field around the crack tip. He used a semi-inverse method developed by Westergaard [16] for solving certain classes of plane strain and plane stress problems. Paris and Sih [14] illustrate this semi-inverse method in detail.

Irwin assumed the material to be a homogeneous, isotropic, elastic solid with an infinitely sharp crack with a straight crack front perpendicular to the specimen surface, (a flat crack). The expressions for the stress field around the crack tip shown in Figure 2.1 are listed as follows:

$$\sigma_x = \frac{K}{\sqrt{2\pi r}} \cos\frac{\theta}{2}\left(1 - \sin\frac{\theta}{2}\sin\frac{3\theta}{2}\right) \qquad (3a)$$

$$\sigma_y = \frac{K}{\sqrt{2\pi r}} \cos\frac{\theta}{2}\left(1 + \sin\frac{\theta}{2}\sin\frac{3\theta}{2}\right) \qquad (3b)$$

$$\tau_{xy} = \frac{K}{\sqrt{2\pi r}} \sin\frac{\theta}{2}\cos\frac{\theta}{2}\cos\frac{3\theta}{2} \qquad (3c)$$

The displacements are:

$$u = \frac{K}{E}(1+\mu)\left(\frac{2r}{\pi}\right)^{1/2} \cos\frac{\theta}{2}\left(1 - 2\mu + \sin^2\frac{\theta}{2}\right) \qquad (4a)$$

$$v = \frac{K}{E}(1+\mu)\left(\frac{2r}{\pi}\right)^{1/2} \sin\frac{\theta}{2}\left(2 - 2\mu - \cos^2\frac{\theta}{2}\right) \qquad (4b)$$

In the development of the above expressions the terms containing r/a have been considered negligible and are neglected. Thus these

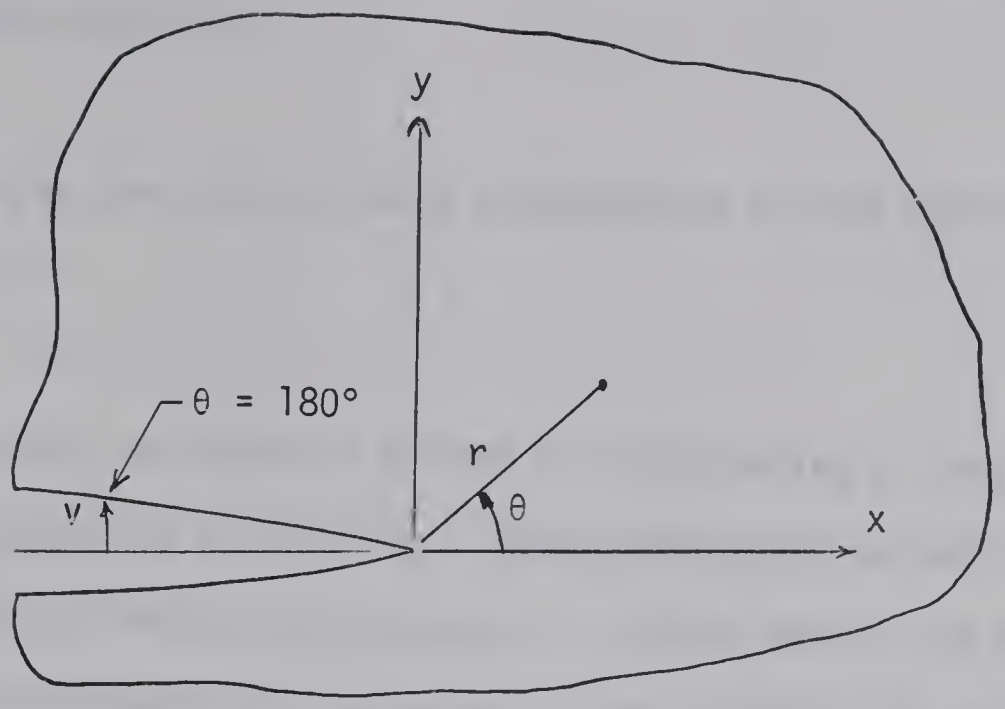

Figure 2.1 Coordinates For the Region Around a Crack Tip

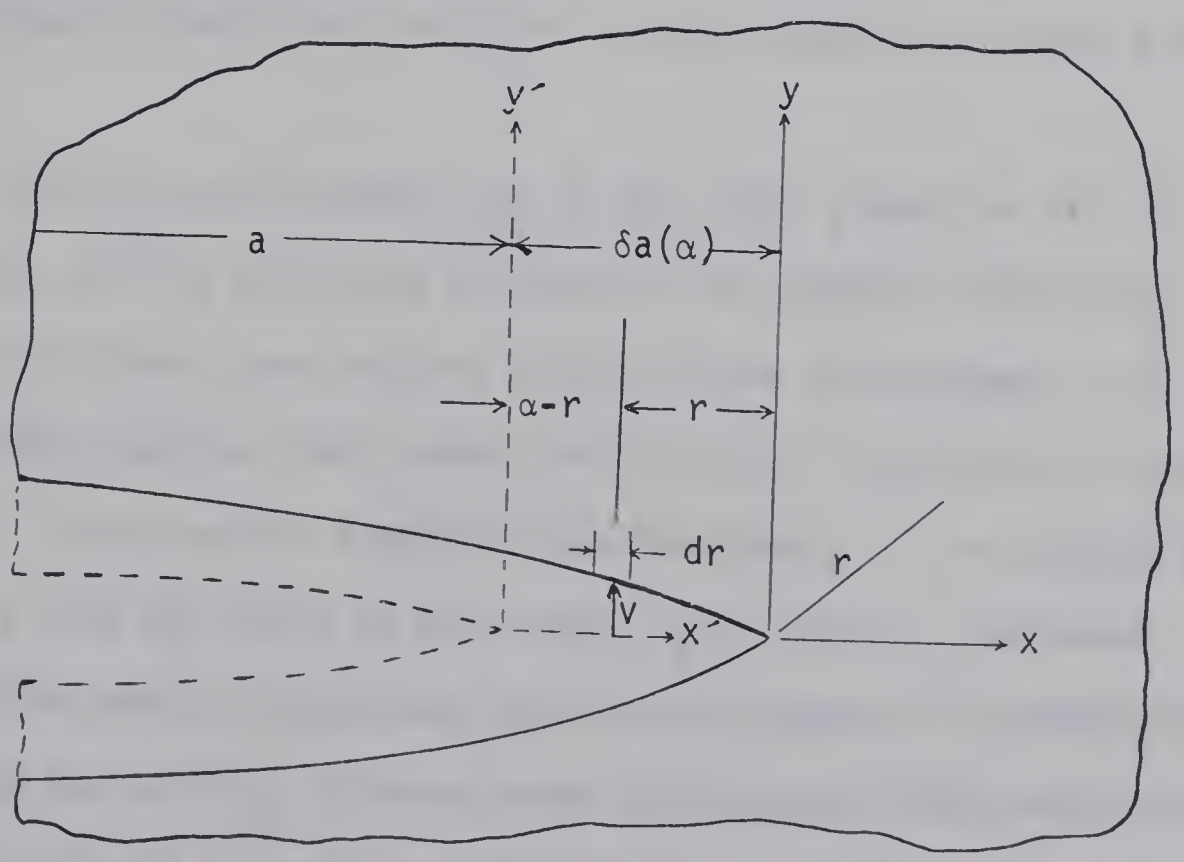

Figure 2.2 Increment of Crack Growth

expressions are for sheet problems and apply only to the region around the crack tip.

2.3 Relating the Strain Energy Release Rate to the Stress Intensity Factor

Irwin [6] introduced a method for calculating G from the elastic stress analysis of a crack tip. Since the region around a crack tip is completely elastic, the decrease in strain energy due to an increment of crack growth, δa, is equal to the increment of work, δW, required to close the increment of crack growth. Consider an elastic body of unit thickness, containing a crack of length a which has been extended by δa as shown in Figure 2.2. Two sets of axis y´x and yx are needed to describe conditions for the cracks of length a and $a + \alpha$.

The loss of strain energy due to the crack growth δa will be restored by pulling the crack surfaces of δa together. The crack surfaces are stress free and the crack surface displacement v is given by the equation (4a), where the distance r is related to the xy origin. Consider the element of surface area, $1 \cdot dr$, moving a distance v with the force on this area, $\sigma_y dr$, where σ_y increases linearly from zero to a maximum, as the displacement is accomplished. The maximum value of σ_y is known from the equation (3a), where the crack is of length a. Note that the displacement v is referred to the xy axis and is a function of the radius r. The maximum value of stress σ_y is referred to the xy´ axis and is a function of the

radius (α-r).

The work required to close the crack (both surfaces) over the distance α is

$$\delta W = 2 \int_0^{\alpha} \frac{\sigma_y v}{2} \, dr \tag{5a}$$

where, σ_y refers to the xy′ axis with $\theta = 0$ and

$$\sigma_y = \frac{K}{\sqrt{\pi(\alpha - r)}}$$

The displacement v refers to the xy axis with $\theta = 180°$ and from equation (4a)

$$v = 2\left(\frac{2}{\pi}\right)^{1/2} \frac{(1-\mu^2)}{E} K r^{1/2} \tag{6}$$

Thus,

$$G\alpha = \delta W \tag{5b}$$

$$\delta W = 2 \int_0^{\alpha} \frac{K^2 \, 2^{1/2}}{E \quad \pi} \left(\frac{r}{\alpha - r}\right)^{1/2} (1 - \mu^2) \, dr \tag{5c}$$

Integrating yields:

$$G\alpha = \frac{2K^2}{\pi} \frac{(1 - \mu^2)}{E} \left[\frac{\alpha\pi}{2}\right] \tag{5d}$$

The relations of the strain energy release rate G in terms of the stress intensity factor for the plane strain state becomes

$$G = \frac{K^2(1 - \mu^2)}{E} \tag{7a}$$

The relation for the plane stress state can be found similarly and is

$$G = \frac{K^2}{E} \tag{7b}$$

As a result of the above development, the strain energy release rate G is also known as the crack extension force.

2.4 Relating the Strain Energy Release Rate to the Compliance of the Test Specimen

Irwin and Kies [5] related the strain energy release rate G to the change of compliance of the specimen. A more general development of the relationship is given as follows.

Consider the specimen shown in Figure 2.3 with an initial load of P_o and crack length a_o. The displacement e, between the loading points increases proportionally with the load as shown in Figure 2.4. Compliance, C, is defined as the displacement e_o divided by the load P_o and is actually the inverse of stiffness.

During an increase of crack length δa the load would decrease an amount δP, and the loading points extend an amount δe. The total strain energy before the crack extension was $P_o C_o$ and after is $(P_o - \delta P)(e_o + \delta e)$. The total change in strain energy, δV, is denoted in Figure 2.4 by the horizontal cross-sectional area minus the angular cross-sectional area. The horizontal cross-sectional area is equal to the increment of work, δW, done on the system, by the external force P. The strain energy released, δaG, due only to the increment of crack

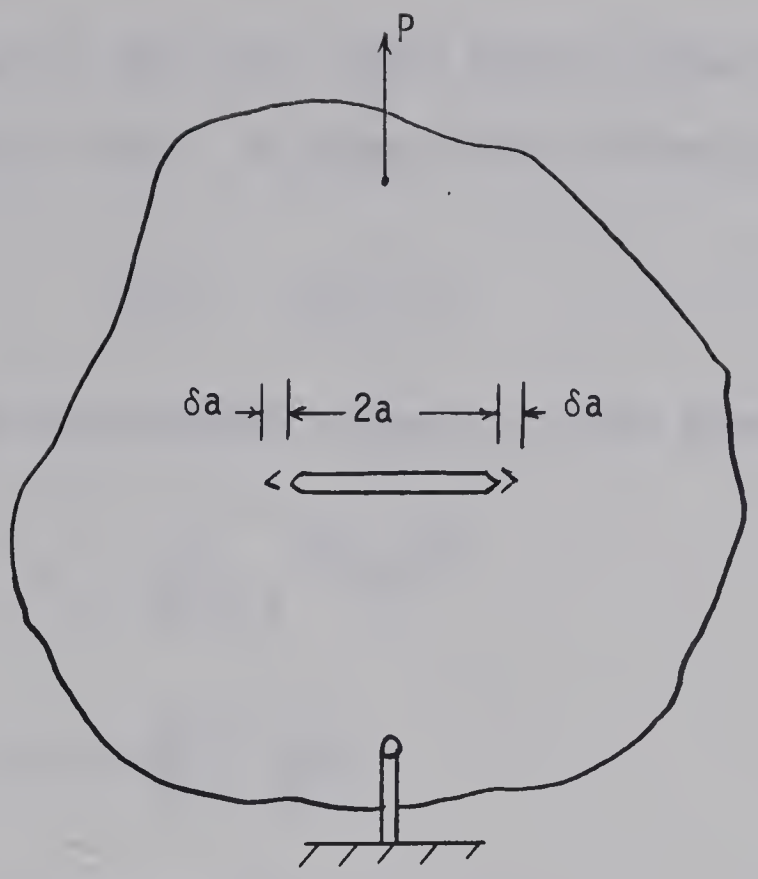

Figure 2.3 Pin Loaded Specimen

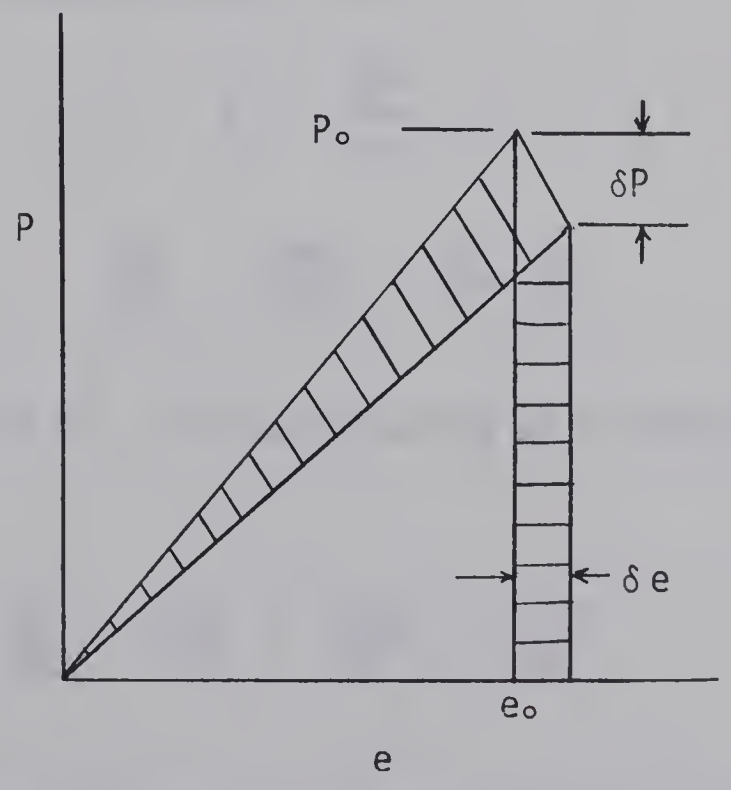

Figure 2.4 Total Strain Energy

growth, δa, is equal to the total strain energy change minus the work done by external forces, as given in the following expression:

$$G\delta a = \delta W - \delta V$$

G is defined for an infinitesimal element of crack growth δa. Thus,

$$G = \lim_{\delta a \to 0} \frac{\delta W - \delta V}{\delta a} \tag{8}$$

or $$G = \frac{dW}{da} - \frac{dV}{da}$$

Total strain energy expression is

$$V = \frac{P_e}{2}$$

Using the compliance relation ($e = CP$),

$$V = \frac{CP^2}{2}$$

$$\frac{dV}{da} = \frac{CP\partial P}{\partial a} + \frac{1P^2}{2} \frac{\partial C}{\partial a} \tag{10}$$

The work term is $\delta W = P\delta e$. Differentiating with respect to crack growth results in:

$$\frac{dW}{da} = \frac{P\partial e}{\partial a} = \frac{PC\partial P}{\partial a} + \frac{P^2\partial C}{\partial a} \tag{11}$$

Substituting equation (10) and (11) in equation (8) yields

$$G = \frac{P^2}{2} \frac{\partial C}{\partial a} \tag{12}$$

Equation (12) indicates that G is independent of small changes in load or loading points, and is dependent only on the changes of specimen compliance for changes in crack length and load. Experimental values of compliance can be used in equation 12 to determine expression for G. The compliance, measured at different crack lengths can be plotted on a graph against the crack lengths. The slope of this plot is used to determine G.

2.5 Corrections for Plasticity Effects

A small zone of yielding is always present at the crack tip. If the plastic zone is "small" and the nominal stress in the specimen is less than eighty percent of the yield stress, the elastic analysis may be applied with small corrections for the crack length [17]. In fracture toughness studies, it has been acceptable to make corrections for the small plastic zone. These corrections also should be applied in fatigue work.

Consider a plastic zone model shown in Figure 2.5 where the yielded region around the crack tip tends to blunt the crack tip. The crack surfaces would move apart with no further crack growth, as suggested in Figure 2.5. The elastic region around the crack tip would "see" an elastic sharp crack tip at a different point than the yielded blunted crack tip. For a blunted crack length of a, the elastic region around the yielded zone would "see" an elastic crack length of $a + r_y$. The elastic stress field in the region, a little distance away from the actual blunted crack tip of length a is the

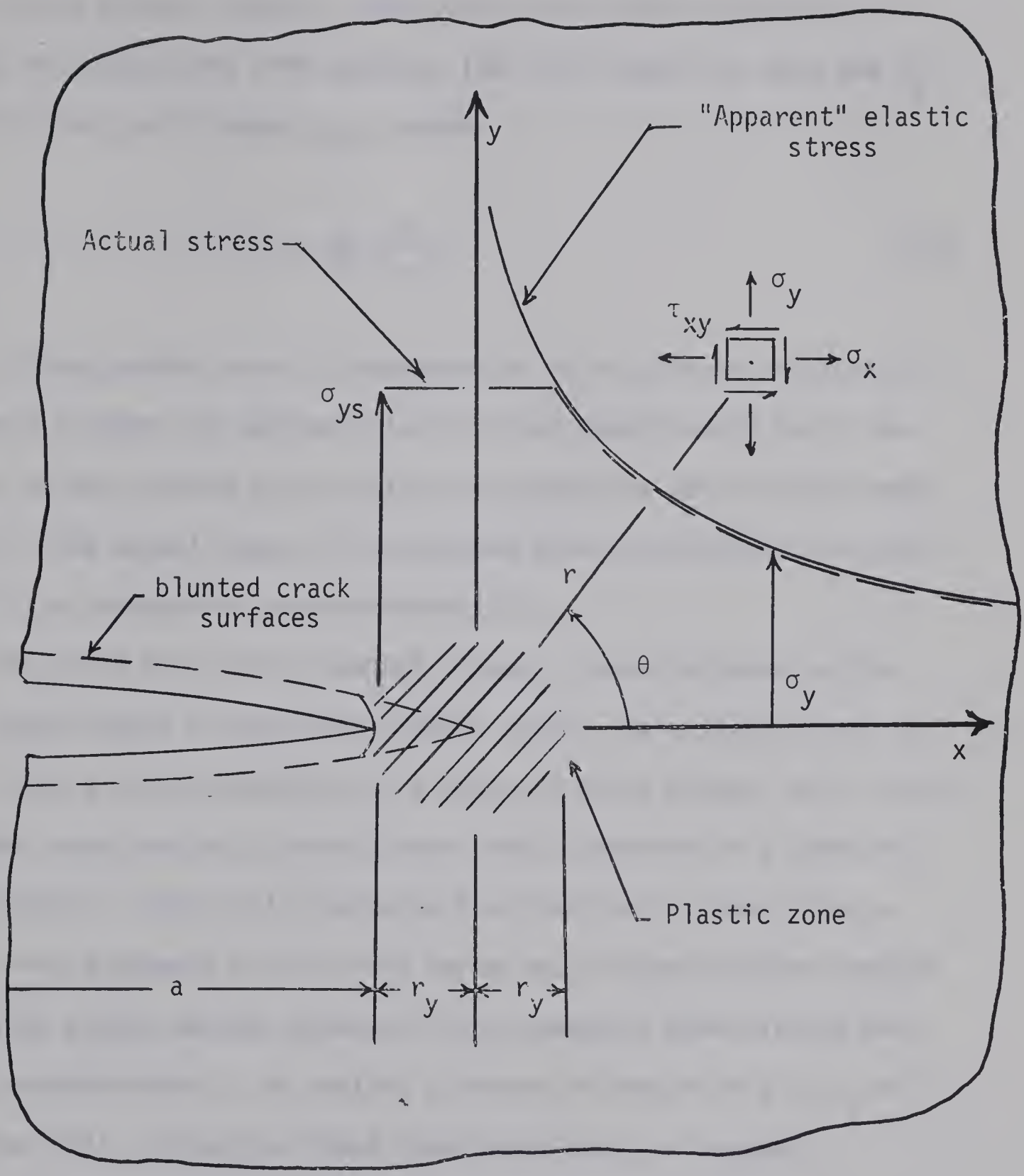

Figure 2.5 Plastic Zone Model

same as that for the ideal elastic crack of length $a + r_y$.

In the elastic analysis, the yield stress would occur at a radius r_y, calculated from equation (3b) for θ equal to zero and σ_y equal to the yield stress, σ_{ys}, where

$$r_y = \frac{1}{2\pi} \left(\frac{K}{\sigma_{ys}}\right)^2 \tag{13}$$

If the yielded zone is considered to be a cylinder as shown in Figure 2.5, then the apparent elastic crack length would be at the center of the yielded zone, making the apparent elastic crack length $a + r_y$. The actual shape of the yielded zone is not known, but this model is an acceptable approximation [17].

The yield stress for aluminum alloys is usually taken as the .2% strain offset of the stress strain curve. This yield stress is taken from a tension specimen in a state of plane stress, which would be lower than the yield stress taken from a specimen in a state of plane strain. Irwin [17] indicated that the plastic zone along a plane strain segment of the crack border may be smaller than that of the plane stress portion because of the change in shear stress and other considerations. He applied a reduction factor of 3 to r_y of equation (13). Hence for plane strain problems, he suggests

$$r_y = \frac{1}{6\pi} \left(\frac{K}{\sigma_{ys}}\right)^2 \tag{14}$$

Crack lengths, measured by the microscope are blunted and must be corrected to equivalent elastic cracks before applying elastic

analysis. The blunted crack length may initially be used to obtain an initial value of K. The plastic zone correction r_y, may be then calculated using equations (13) or (14) and the apparent elastic crack may be found. An iterative procedure may be used to determine K.

2.6 Fatigue Crack Propagation

Fatigue has been defined as fracture under cyclic loading and is the most common cause of service failures [10]. A fatigue failure can be thought to have three stages: initiation, propagation, and a final unstable failure. Initiation is the period required for a crack to start growing from a micro crack or structural flaw to a propagating crack. In the second stage the crack grows slowly and almost continuously due to the cyclic loading. The final stage is rupture due to an unstable running crack and/or ductile yielding.

Various approaches have been used to explain the crack propagation stage, resulting in an abundance of crack propagation laws. Paris and Erdogan [18] in 1964 did a critical analysis of the more acceptable crack propagation laws and their approach agreed better than the other crack propagation laws for a wide range of test data. Paris and Erdogan proposed that the crack propagation rate should be a particular function of the stress intensity factor for a particular material. A plot of the logarithm (ΔK) versus the logarithm (da/dN) was used to show that there was general agreement for the law,

$$\frac{da}{dN} \alpha(\Delta K)^4 \qquad (15)$$

The more recent paper, Hertzberg and Paris [19] uses the stress intensity approach along with the results of electron fractography studies in studying crack propagation. They showed that the striations observed by the electron microscope had almost the same correlation with ΔK, as the crack propagation rate on log-log plots. In crack propagation studies, there is not substantial agreement of ΔK versus da/dN correlations from different sources. The log (ΔK) versus log (da/dN) plot minimizes the differences of the data so a single line may be drawn through the data. One reason for the differences is that many factors which affect the crack propagation rates are not accounted for by the single parameter ΔK. The stress intensity factor, ΔK, is based only on the value of the cycling stress and specimen geometry. Other factors affecting the crack propagation rate are the stress ratio (R), type of the waveform of the cyclic load, frequency of the cycling load, size of specimen (thickness), temperature, and even such things as the humidity of the test room.

Roberts and McEvily [20] have plotted log (ΔK) versus log (da/dN) for various values of R. They concluded that the crack propagation rate is a function of ΔK and R as follows:

$$\frac{da}{dN} \propto (R)^{-2} (\Delta K)^{4} \tag{16}$$

2.7 Application of Theory to Test Data

The change in compliance due to the crack was found experimentally for 25 to 50 crack lengths varying from 0 to 1.7 inches on the 3.5 inch

wide SEN specimen. The strain energy release rate G, was found from the compliance measurements using equation 12:

$$G = \frac{P^2}{2} \frac{dC}{da}$$

where P is the applied force per unit thickness, and C is the total compliance of the specimen per unit thickness. It is convenient to express this relationship in the dimensionless form

$$\frac{EwG}{P^2} = \frac{E}{2} \frac{dC}{da/w} \qquad (17)$$

The dimensionless form of the strain energy release rate as in equation (17) may be correlated with the relative crack length a/w. This correlation will apply to specimens of any material or size, providing the length-width ratio of specimens are within certain limits.

In calculating the stress intensity factor from the strain energy release rate, there is a question of whether the two-dimensional plane stress or plane strain analysis may be used for test specimens. The state of stress in a cracked plate specimen is one of plane stress, except within a very restricted region of the crack where the constraining influence of the crack induces a stress state approaching plane strain. The crack surface and the region near the center of the crack tip is considered to be in plane strain state for lower values of K and flat cracks. The plane stress state appears to start at the surface of the specimen with the formation of a shear lip. The shear lip gradually moves across the crack tip to the center of the specimen for increased values of K. It is generally agreed that once the surface of the crack attains a slope of 45 degrees, the region around the

crack tip is in a state of plane stress. Irwin [21] has discussed the question of plane stress or strain for fracture toughness tests. Hertzberg and Paris [19] use some of Irwin's arguments to discuss fatigue. The stress intensity factor has been calculated for both plane stress and plane strain using equations (7a) and (7b). The factor K has been developed for a perfectly elastic material and since a plastic zone is always present at the crack tip, the apparent elastic crack lengths must be calculated.

In these experiments, a microscope was used to measure the surface crack lengths. The plastic zone correction, r_y of equation (13) was added to the surface crack lengths for the plane stress problem. For the plane strain problem, the crack length at the center of the crack front was obtained by adding the correction for the parabolic shape of the crack front to the surface crack length. The correction was found to be zero at the start of the fatigue crack and increased to maximum value of 0.005, 0.007, and 0.009 inches at the end of the tests for specimen thicknesses of 0.050, 0.080 and 0.126 inches respectively. The plastic zone correction of equation (14) was added to the center crack lengths for the plane strain problem.

Since K depends on the crack length and the crack length correction depends on K, an iterative process was used to calculate K. The stress intensity factor was calculated using the original measured crack lengths. The plastic zone corrections were calculated using the initial K value and applied to the crack lengths. A new K was then calculated using the corrected crack lengths. The process was repeated until it was evident that no further iterations were necessary.

The plot of compliance measurements versus relative crack length were fitted to a polynomial expression of a/w of degrees 3 to 10 by means of a least-square-best-fit digital computer program. The resulting expression was:

$$E\Delta C = \frac{A_1}{2}\left(\frac{a}{w}\right)^2 + \frac{A_2}{3}\left(\frac{a}{w}\right)^3 + \frac{A_3}{4}\left(\frac{a}{w}\right)^4 + \ldots + \frac{A_n}{n+1}\left(\frac{a}{w}\right)^{n+1}$$

$$\text{for } n = 4, 5, \ldots, 10 \qquad (18)$$

The constant and first power of a/w were not included in the expression because the strain energy release rate is zero for zero crack length. The criteria for optimum fit [22] was taken to be the sum of the residuals squared, divided by the degree of freedom m - k - 1, where m is the number of points and k is the number of terms in the polynomial. This error variance indicates that polynomials of degrees 3 to 5 were usually as good as higher degree polynomials for the single precision computer program.

Using equations (7b), (12), (13), and (18) the stress intensity factor for the plane stress was found from compliance measurements and was put in the following form:

$$K = \frac{\sigma\sqrt{w}}{2}\left[A_1\frac{a_c}{w} + A_2\left(\frac{a_c}{w}\right)^2 + \ldots + A_n\left(\frac{a_c}{w}\right)^n\right]^{1/2} \qquad (19)$$

where

$$a_c = a + \frac{1}{2\pi}\left(\frac{K}{\sigma_{ys}}\right)^2 \qquad (20)$$

and stress intensity factor for the plane strain case is:

$$K = \frac{\sigma\sqrt{w}}{2(1-\mu^2)}\left[A_1\frac{a_c}{w} + A_2\left(\frac{a_c}{w}\right)^2 + \ldots + A_n\left(\frac{a_c}{w}\right)^n\right]^{1/2} \qquad (21)$$

where $a_c = a + \frac{1}{6\pi}\left(\frac{K}{\sigma_{ys}}\right)^2$ + curvature correction. (22)

The above equations are presented graphically in Chapter 4.

CHAPTER III

EXPERIMENTAL TEST METHODS

3.1 Test Specimen

The material used in this investigation was bare aluminum alloy 2024-T3 which is one of the common materials used in crack propagation studies [2, 19, 20]. Hence a comparison of results can be made quite easily. The clad material 2024-T3 is presently used in large commercial quantities, but the bare 2024-T3 was chosen because of the effects the soft cladding may have on crack propagation results. The mechanical properties of the material listed in Table I were obtained from the tension specimen shown in Figure 3.1.

The SEN specimens shown in Figure 3.2 were cut from three sheets of material of thicknesses 0.050, 0.080, and 0.125 inches. They were cut using a milling cutter with the direction of rolling parallel to the applied stress and perpendicular to the path of the propagating crack. The length to width ratio for SEN specimens should be greater than four. Srawley, Jones, and Gross [15] found no significant differences between K curves obtained from specimens with a length to width ratio of four and specimens with a length to width ratio of eight. Compliance readings for these specimens are shown in Figure 4.4 Compliance readings on the 24 inch specimen were about three percent lower than those of the 12 inch specimen. This difference was not considered to be significant.

TABLE I

Mechanical Properties of Bare 2024-T3

Mechanical Properties of Aluminum Alloy	Test Specimen Thickness 0.05 Inches	0.080 Inches	.125 Inches
σ_y (.2% Offset) k.s.i.	55.5	52.0	57.
σ (ultimate) k.s.i.	71.5	67.8	74.8
E k.s.i.	10,200	10,360	10,300
μ	.320	.326	.325
% elongation (6 inch gauge length	22.1	21.2	11.0

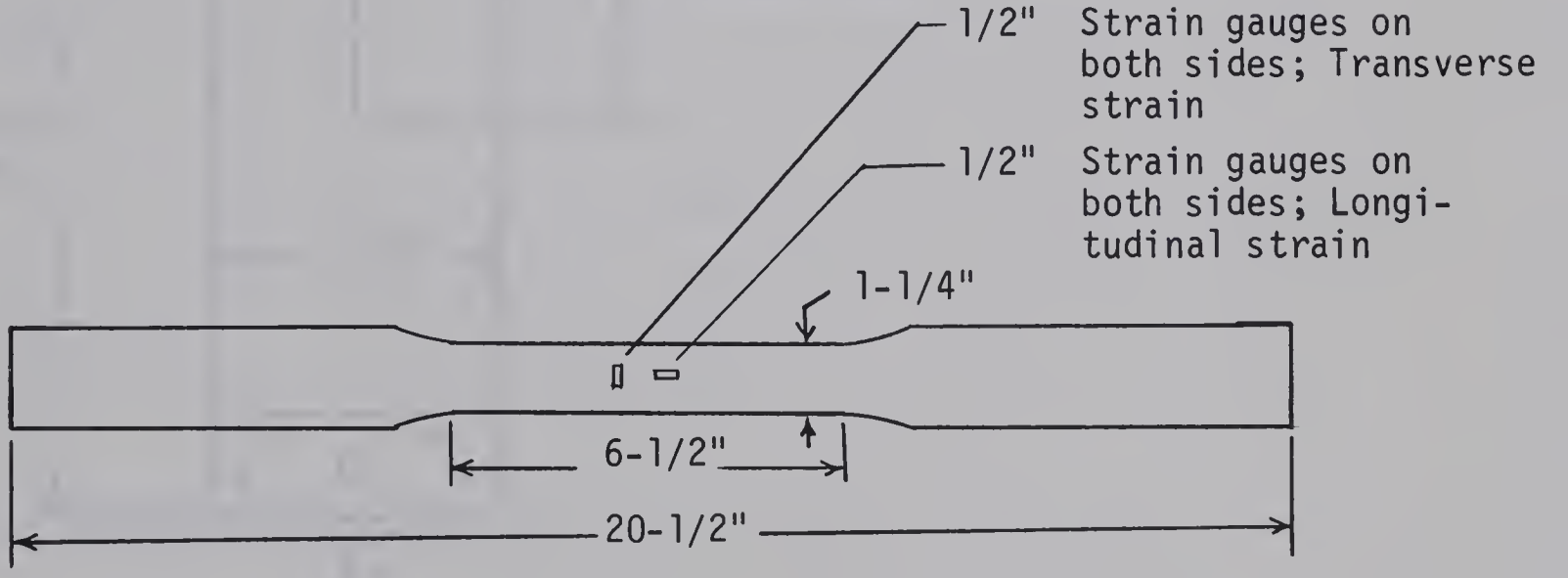

Figure 3.1 Tension Test Specimen

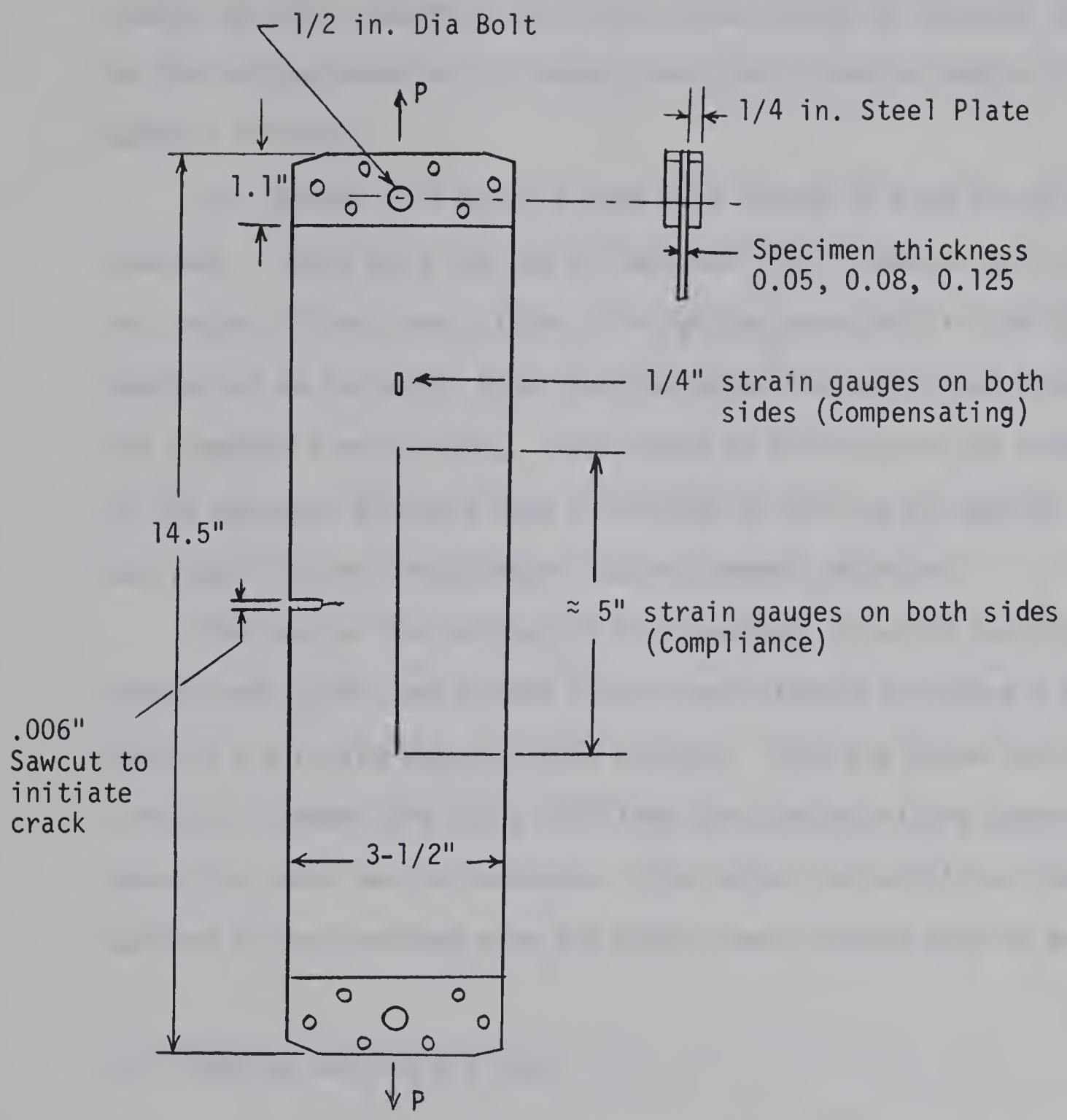

Figure 3.2 SEN Specimen

An ASTM Special Committee [23] recommended types of holding blocks for test specimens, but the limited length of testing space in the fatigue machine (15 inches) required a special design of holding fixtures.

Two quarter inch steel plates were bolted to each end of the specimen. Loads were applied by two, half inch diameter bolts through the center of the steel plates. The plates were held in the fatigue machine so as to permit free rotation about the bolts, but preventing the specimen from twisting. The effect of friction on the rotation of the specimen may have been eliminated by the use of special bearings, but this requirement was not deemed necessary.

The area of the surface of the specimen, to which the strain gauges were glued, was sanded lightly and cleaned to insure a good bond of the strain gauges to the surface. Care was taken not to scratch or remove the oxide film from the surface of the specimen where the crack was to propagate. The darker oxide film on the surface of the specimen made the shiny crack surface easy to see.

3.2 Testing Machine and Room

A Sonntag Universal Fatigue Testing Machine, Model SF-1-U, with an alternating load frequency of 1800 cycles per minute was used. Calibration tests indicated a static load error less than three percent of load or one-half percent of the total capacity. There were other sources of errors in loads besides the errors indicated in calibration tests. The static load was set manually at the start of each test. The static load changed only slightly

during the test because of the compliance changes of the specimen, thus the static load was not reset during the test. A deflection of the head fixtures of the testing machine was noted when the dynamic load approached the capacity of the machine. The magnitude of the load errors due to the deflection of the head fixture and the manual load setting were unknown but these should not be significant.

The testing machine was located in a room without air-conditioning. The tests were carried out in June and July with the temperature remaining fairly constant, with a maximum of 80 degrees and a minimum of 73 degrees during testing. The relative humidity was found using a wetbult thermometer, and remained between 25 to 45 percent during all tests. Although the temperature and humidity were not controlled, daily variations were within two degrees of temperature and five percent humidity. These daily variations were considered small and would not make any significant differences in the tests.

3.3 Test Loads

A maximum stress, based on the gross cross-sectional area, of 4.5 ksi and a stress ratio, R, equal to .2 was applied to all specimens. An alternating stress of 3.6 ksi was chosen so the crack would propagate across the specimen in a reasonable time (4 to 6 hours). The minimum stress was set as low as possible so the value of ΔK would be close to the value of K. A minimum stress of .9 ksi was chosen because as the minimum stress approached zero, the load wave form was deformed and noise or chatter resulted because of loose fittings and slackness in the

machine. To prevent slow yielding at the crack tip due to the static load, the cyclic load was not stopped during the crack propagation stage of the tests.

3.4 Strain Gauge Instrumentation

Strain gauges were connected in such a fashion that only the change in strain due to the presence of a crack was recorded. Five inch, single wire strain gauges of 120 ohms (compliance gauges), were placed in the center of the specimens which measured the average longitudinal strain in the cracked section. A compensating gauge of a quarter inch gauge length and 120 ohms was placed near the end of the specimen to measure the average longitudinal strain in the uncracked section of the specimen.

The compensating and compliance strain gauges were placed on each side of the sheet specimen, so that an average value of the strain measurement was obtained. The compensating gauges were placed in opposite arms of a wheatstone bridge circuit while the compliance gauges were in the same circuit such that only the increase in strain due to the presence of the crack was measured. Thus the output of the wheatstone bridge circuit was twice the increase of strain due to the crack. A variation in the average longitudinal stress did not effect the compliance measurement because the average longitudinal strain was compensated for in the wheatstone bridge circuit.

Srawley, Jones, and Gross [15] suggest that the gauge length should be four times the length of the longest crack in the SEN

specimen. Since the gauge length of five inches is not four times the longest crack considered (1.55 inches), a slight error may have resulted. Errors in positioning the long strain gauges in the center of the specimen should be insignificant. The notch, being only on one side of the SEN specimen, and pin loadings caused the SEN specimen to bend under load. Consequently the long strain gauges will be slightly curved. Srawley, Jones, and Gross [15] measured the bending and found it to be "small". Thus no significant error should result in compliance measurements due to this slight curvature of the long strain gauges.

An SR-4 Strain Indicator and an oscilloscope with a "Q" unit was used to analyze the output of the strain gauges. The SR-4 Strain Indicator measured the mean value of the dynamic strain at the center of the specimen due to the crack. The accuracy of the SR-4 Strain Indicator was adequate for compliance calculations, whereas the accuracy of the oscilloscope was not. The oscilloscope was used to show the dynamic strain waveform as a check for any distortion or resonance of the strain waveform. This was necessary because in some preliminary tests, the dynamic strain waveform became distorted and an increase in magnitude of the dynamic strain of up to 25 percent occurred for a SEN specimen of dimensions 0.05 x 22 x 4 inches over a relative crack length of 0.35 to 0.415. In the tests used for compliance measurements, only the 0.125 inch thick specimen showed a similar distortion. The distortion was noted only for a short interval of crack growth, thus there should be not significant effect on crack propagation results.

3.5 Crack Length Measurement

A measuring microscope was used to both observe the crack tip, and to measure the crack length to a precision of a thousandth of an inch. A 30 power microscope was used in initial tests and a 40 power microscope used in later tests made the crack tip easier to define. The crack tip could not always be seen, thus there was a possible human error present in defining the location of the crack tip. Erdogan and Roberts [20] found the sensitivity of a 50 power microscope was higher than the accuracy with which the crack tip could be defined, as some contraction in thickness at the crack tip was observed. Thus a higher power microscope may have eliminated errors in defining the crack tip.

A stroboscope allowed the crack to be observed in the fully opened or closed states. The crack tip could be observed best when the surface of the specimen was left in the oxidized state with a minimum of scratches. When the crack was in the fully opened state, the flashing light made the shiny surface of the crack easy to see against the darker oxidized surface of the specimen.

In several of the preliminary tests, the alternating load was stopped and india ink injected into the crack near the crack tip. The ink was allowed to dry in the crack before applying the alternating load. Upon complete failure of the specimens, the shape of the crack front could be seen at the various crack lengths where the ink had been injected and dried.

Observations from these preliminary tests were used to calculate the crack lengths at the center portion of the specimen.

CHAPTER IV

TEST RESULTS AND DISCUSSION

4.1 Compliance and Stress Intensity Factor Curves

The original test data, that is the compliance measurements and surface crack lengths, is presented in tabular and graphical form. The stress intensity factors are presented in graphical form for comparison. The differences of the results are discussed with respect to different characteristics of the tests and possible sources of error.

The set of crack lengths, compliance readings, and number of loading cycles are recorded for six tests in Tables II to VII. The first five crack lengths are sawcuts of approximately 0.006 inches in width and the remaining are fatigue crack lengths. The compliance readings for the sawcuts provide points on the curves below a relative crack length of 0.2. The useful region for fatigue testing on the SEN specimen is between 0.2 and 0.5 relative crack lengths. The compliance readings and relative crack lengths are plotted for the tests in Figures 4.1, 4.2, and 4.3. To avoid confusion, only about one half of the readings given in the tables are shown in the figures.

The compliance readings for several tests of Srawley, Jones, and Gross [15] are shown in Figure 4.5. They used the average compliance readings for two, twelve inch long specimens to calculate G and to be used for publication in later papers [24]. The average

compliance readings of these two specimens are used for comparison in Figures 4.1, 4.2, and 4.3. The difference between tests and the scatter in each test are probably the result of errors in crack length measurements, errors in compliance readings, and the fatigue crack changing from a flat to a slanted crack.

Compliance readings for several tests had to be disregarded because of errors due to the binding of specimens in the holding blocks and large temperature difference during tests. The accuracy of the travelling microscope was adequate for accurate crack length measurements. A small error may be present in crack length measurements due to the difficulty of seeing the exact location of the crack tip, but would not exceed one hundredth of an inch. From the tabulated data, it can be seen that the load was applied a few thousand times before a notch was cut. This initial loading served as a shakedown period, required to get stable compliance readings for a zero crack length. All the compliance readings were taken when the specimen was under the dynamic load as there was an unexplainable difference between the compliance reading of the mean dynamic load and the compliance reading of the static load. The difference was fairly constant for the entire test. A total of twenty-one SEN specimens were tested. Most of the preliminary tests had large errors in the compliance readings. Changes in the experimental methods such as; use of compensating gauges, use of a stroboscope, control of temperature, and accurate setting of end fixtures eliminated most of the errors. As seen from the scatter of points and differences for tests on identical specimens, there must still be small errors.

The least squared error method was used to fit the compliance versus relative crack length curves to polynomial expressions as discussed in Section 2.7. The stress intensity factor curves obtained from the compliance curves are shown in Figures 4.5 to 4.10 for specimens of thickness 0.050, 0.080, and 0.125 inches. The stress intensity factor curves for the plane stress problem as calculated from Srawley, Jones, and Gross' [15] work is shown on each figure for comparison. Their K curve is also shown for the plane strain condition, as well as the plane stress condition in Figure 4.11. Comparing the curves over a relative crack length 0.2 to 0.45, tests numbered 1, 3, 4, and 6 are slightly above Srawley, Jones, and Gross' curves; whereas tests numbered 2 and 5 are slightly below those of Srawley, Jones, and Gross. From these observations, it appears that the K curve of Srawley, Jones, and Gross is applicable to fatigue cracks in SEN specimens if the plastic zone correction factor is applied to the fatigue crack length.

An example of the effect of the plastic zone correction on K can be obtained from Figure 4.12 which shows K calculated with and without the plastic zone and crack curvature corrections. There is a significant shift of the K curve without the use of this correction. There are no notable differences in the curves for specimens of different thicknesses. In all test curves, except test number 4, the value of the stress intensity factor increased slightly in relation to that of Srawley, Jones, and Gross, as a relative crack length of 0.45 was approached. The slant of the crack surface increased as the relative crack length increased.

This is ullustrated in Figure 4.13. The slanting crack surface is the only observed factor that could possibly cause the increased value of K relative to the value of K as obtained by Srawley, Jones and Gross. This increase would not amount to five percent, thus it is not too significant.

4.2 Transition of Crack Surfaces

The cross-sections of test specimens are shown in Figure 4.13 for various relative crack lengths. The fatigue crack surface is initially flat at the start of the fatigue crack and slanted near the center of the specimen. The surface changes by the formation of a "shear lip" growing from the surface of the specimen across the crack to the center, at which time the crack surface would be at a fairly constant slope of about 20 degrees. In earlier tests, the stress ratio (R) was larger and a slope of about 38 degrees was obtained. As seen from Figure 4.13 the slope does not change uniformly. In the thinner specimens (0.050 inches thick), the slanted surface developed rather "fast" and shifted back and forth. In the thicker specimens (0.125 inches thick), the slanted surface developed slowly and more uniformly.

At times a "V" crack surface developed rather than a slanted surface. The "V" crack caused the crack to deviate from the straight crack path in a direction opposite to the point of the "V".

Irwin [21] has studied the transition of the crack surface for fracture toughness tests. He found from equations 3a, 3b, and 3c that the distance r from the crack tip at which the predicted tensile

stress equals the yield stress, is greatest at $\theta = 60$ degrees where

$$r = \frac{0.84}{\pi} \frac{K^2}{\sigma_{ys}^2} \tag{23}$$

When the plate thickness B, was equal to twice r of equation 23, Irwin concluded that the transition of the crack from flat to slant was beginning. That is

$$B = 2r \quad \text{and} \tag{24}$$

$$K = \frac{\sqrt{B\pi}\sigma_{ys}}{\sqrt{1.68}} \tag{25}$$

He showed that there was good agreement for the results of fracture toughness tests. Applying equations 24, 25, and K curves to test specimens, the relative crack lengths at which the surface transition would occur should be 0.35, 0.38, and 0.45 for specimens of thickness 0.050, 0.080, and 0.125 inches respectively. As seen in Figure 4.13 the transition occurs at smaller relative crack lengths.

Hertzberg and Paris [19] use the same reasoning as Irwin [21] for transition of fatigue cracks on thinner specimen except that

$$r = \frac{K^2}{2\pi(\sigma_{ys})^2} \quad \text{and} \tag{26}$$

$$K = \sqrt{\pi B}\, \sigma_{ys} \tag{27}$$

They found the K of equation 27 occurred approximately at the point when the flat fracture was completely eliminated. Using this reasoning, the transition should occur at relative crack lengths of 0.28, 0.32, and 0.41 for 0.050, 0.080, and 0.125 inch thick specimens, respectively. These crack lengths agree better than those obtained from equation 25 for the cross section on Figure 4.13.

4.3 Validity of the Stress Intensity Factor

The stress intensity factor was obtained from the strain energy release rate. This rate is developed from energy concepts for cracks with no restrictions as to a perfectly elastic or plastic solid, or a slanted or flat crack. The stress intensity factor has been developed for a flat crack in a perfectly elastic solid under conditions of plane stress or plane strain. The G expressions obtained for the test specimens are completely correct according to the definition of G. The K expressions obtained for the fatigue cracks are not correct according to the assumptions for which K was defined. The effects of the plastic zone has been approximately corrected for when calculating K but no correction could be applied for the slanting of the crack tip.

A slant crack tip is under a shear and tension loading. Stress intensity factors have been developed for shear and tension loads on flat crack tips and could possibly be related to slanted cracks. Paris and Sih [14] have related G to K for a shear load in a manner similar to that relating G to K for a tension load as in Section 2.4. Since only one value of G was found experimentally, there is no way of knowing what portion of G would be due to the shear loading or to the tension loading for a slanted crack. The K defined for tension loadings has been accepted as a parameter that is correlated with the crack propagation rate [19, 20], but it should be kept in mind that this K is not an accurate description of the stress fields for a slanted crack but may occasionally be encountered.

TABLE II

Experimental Data for a 0.050 Inch SEN Specimen

Test No. 1

Number of load cycles 1000's	Crack length in.	EΔC	Number of loading cycles 1000's	Crack length in.	EΔC
20	0	0	250	.969	.446
21	.12	.016	255	.987	.462
22	.23	.030	260	1.003	.487
22	.37	.056	265	1.032	.515
23	.50	.096	270	1.048	.554
24	.635	.142	275	1.075	.583
72	.648	.153	280	1.095	.616
80	.656	.158	285	1.118	.656
90	.665	.156	290	1.143	.715
100	.679	.172	295	1.179	.783
110	.694	.178	300	1.204	.819
120	.704	.184	305	1.238	.916
130	.715	.195	309	1.259	.990
140	.734	.200	313	1.301	1.066
150	.752	.219	316	1.328	1.150
160	.765	.233	319	1.355	1.236
170	.788	.249	322	1.385	1.335
180	.800	.263	325	1.424	1.460
190	.826	.285	328	1.465	1.610
200	.848	.298	331	1.505	1.811
210	.865	.318	334	1.560	2.101
220	.882	.353	336	1.610	2.319
230	.909	.372	338	1.64	2.801
240	.940	.400	339	1.67	
245	.956	.425	341	1.71	
			342	1.75	
			343	1.85	
			344	Failed	

TABLE III

Experimental Data for a 0.050 Inch SEN Specimen

Test No. 2

Number of load cycles 1000's	Crack length in.	EΔC	Number of loading cycles 1000's	Crack length in.	EΔC
50	0	0	235	.946	.394
50	.12	.016	245	.988	.443
50	.23	.019	250	1.003	.475
50	.37	.042	255	1.032	.496
50	.49	.081	260	1.067	.550
56	.617	.136	265	1.082	.575
95	.627	.147	270	1.112	.609
105	.638	.147	275	1.140	.660
115	.654	.151	280	1.182	.745
125	.669	.159	284	1.213	.785
135	.686	.173	288	1.250	.853
145	.702	.189	292	1.283	.956
155	.722	.202	296	1.327	1.160
165	.737	.205	300	1.373	1.222
175	.765	.218	303	1.411	1.346
185	.794	.250	306	1.462	1.50
195	.815	.269	308	1.494	1.63
205	.844	.296	310	1.542	1.80
215	.880	.322	312	1.587	2.05
225	.908	.338	313	1.612	2.20
			314	1.629	2.30

TABLE IV

Experimental Data for a 0.080 Inch SEN Specimen

Test No. 3

Number of load cycles 1000's	Crack length in.	EΔC	Number of loading cycles 1000's	Crack length in.	EΔC
33	.00	0	240	.999	.512
33	.09	.013	245	1.020	.537
37	.19	.024	250	1.030	.562
41	.31	.046	255	1.048	.594
46	.40	.075	260	1.068	.620
50	.51	.101	265	1.097	.675
54	.59	.148	270	1.138	.742
90	.623	.156	275	1.165	.798
110	.653	.181	280	1.196	.865
124	.675	.203	285	1.241	.976
135	.701	.214	287	1.278	1.100
140	.713	.220	291	1.316	1.182
150	.725	.238	294	1.351	1.278
160	.745	.249	297	1.379	1.390
170	.761	.268	299	1.409	1.521
180	.790	.290	300	1.429	1.588
190	.820	.312	302	1.454	1.675
200	.847	.353	303	1.471	1.791
205	.872	.364	306	1.55	
210	.888	.386	314	1.9	
215	.903	.404			
220	.925	.428			
225	.937	.441			
230	.959	.462			
235	.974	.485			

TABLE V

Experimental Data for a 0.080 Inch SEN Specimen

Test No. 4

Number of load cycles 1000's	Crack length in.	EΔC	Number of loading cycles 1000's	Crack length in.	EΔC
19	0	0	245	1.013	.530
20	.1	.013	250	1.039	.567
21	.25	.033	255	1.067	.655
22	.375	.063	260	1.105	.675
23	.49	.098	265	1.138	.739
26	.605	.140	270	1.170	.835
70	.610	.142	274	1.205	.904
80	.616	.151	278	1.228	.981
90	.625	.156	282	1.290	1.110
100	.631	.162	285	1.329	1.211
111	.650	.169	288	1.375	1.328
120	.657	.180	291	1.415	1.491
130	.678	.202	294	1.472	1.710
140	.695	.208	297	1.526	1.930
150	.716	.219	300	1.620	2.161
160	.734	.230	304	1.75	
170	.758	.249	305	1.85	
180	.780	.271			
190	.805	.293			
200	.828	.322			
210	.863	.348			
220	.889	.383			
230	.934	.427			
235	.959	.461			
240	.993	.497			

TABLE VI

Experimental Data for a 0.125 Inch SEN Specimen

Test No. 5

Number of load cycles 1000's	Crack length in.	EΔC	Number of loading cycles 1000's	Crack length in.	EΔC
35	0	0	206	1.141	.659
40	.012	.016	209	1.185	.714
45	.022	.024	212	1.220	.765
50	.036	.057	214	1.249	.816
55	.050	.093	216	1.290	.912
56	.062	.128	219	1.339	1.072
99	.65	.131	222	1.384	1.190
109	.676	.145	223	1.411	1.285
119	.693	.166	225	1.464	1.462
129	.721	.184	227	1.511	1.685
139	.753	.205	228	1.554	
149	.784	.230	229	1.602	
159	.813	.255	230	1.65	
169	.874	.301	230.5	1.75	
179	.927	.348	231	1.90	
184	.945	.386			
189	.984	.427			
194	1.024	.473			
200	1.088	.576			
203	1.106	.615			

TABLE VII

Experimental Data for a 0.125 Inch SEN Specimen

Test No. 6

Number of load cycles 1000's	Crack length in.	EΔC	Number of loading cycles 1000's	Crack length in.	EΔC
49	0	0	185	.962	.428
50	.12	.011	190	.994	.468
51	.24	.030	195	1.027	.523
52	.38	.065	200	1.067	.595
56	.612	.156	203	1.102	.635
62	.612	.136	206	1.129	.687
98	.623	.145	209	1.148	.741
108	.669	.156	212	1.190	.823
119	.675	.181	215	1.225	.872
129	.706	.194	218	1.272	1.015
139	.740	.206	220	1.300	1.090
149	.777	.240	222	1.335	1.190
159	.815	.277	224	1.384	1.380
170	.869	.324	226	1.435	1.582
180	.926	.383			

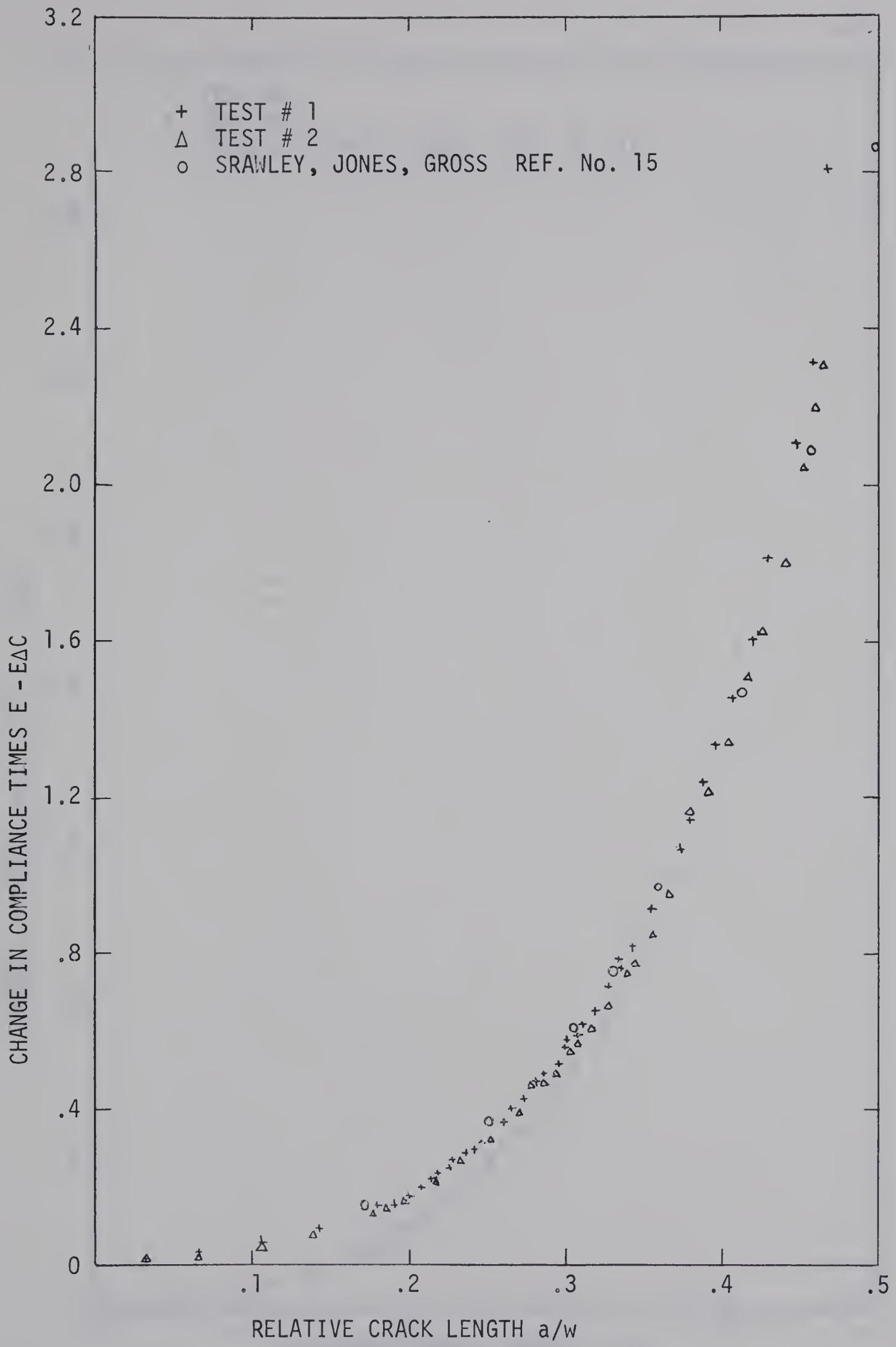

Figure 4.1 Compliance Curve for 0.060 inch Thick SEN Specimen

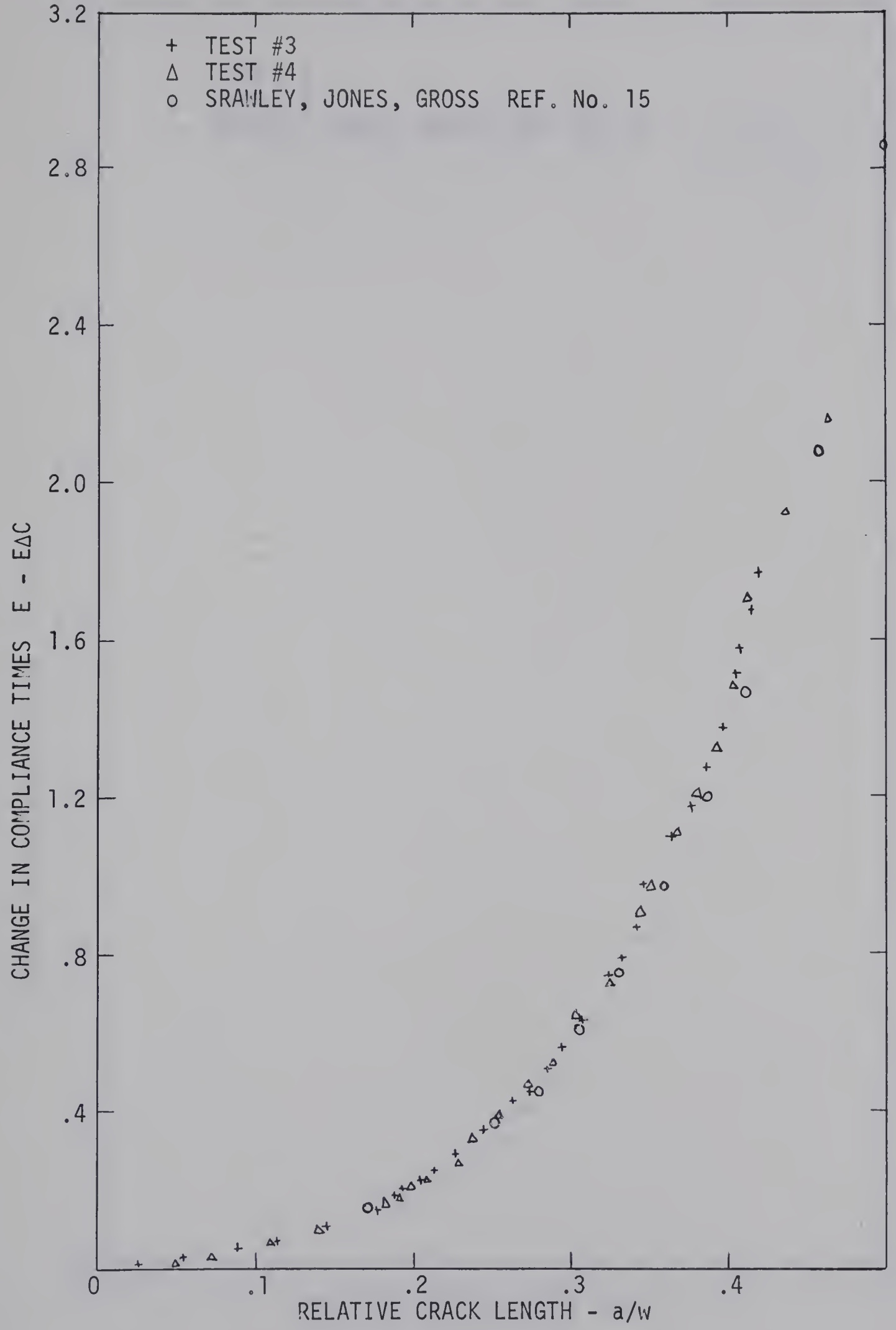

Figure 4.2 Compliance Curves for 0.080 Inch SEN Specimen

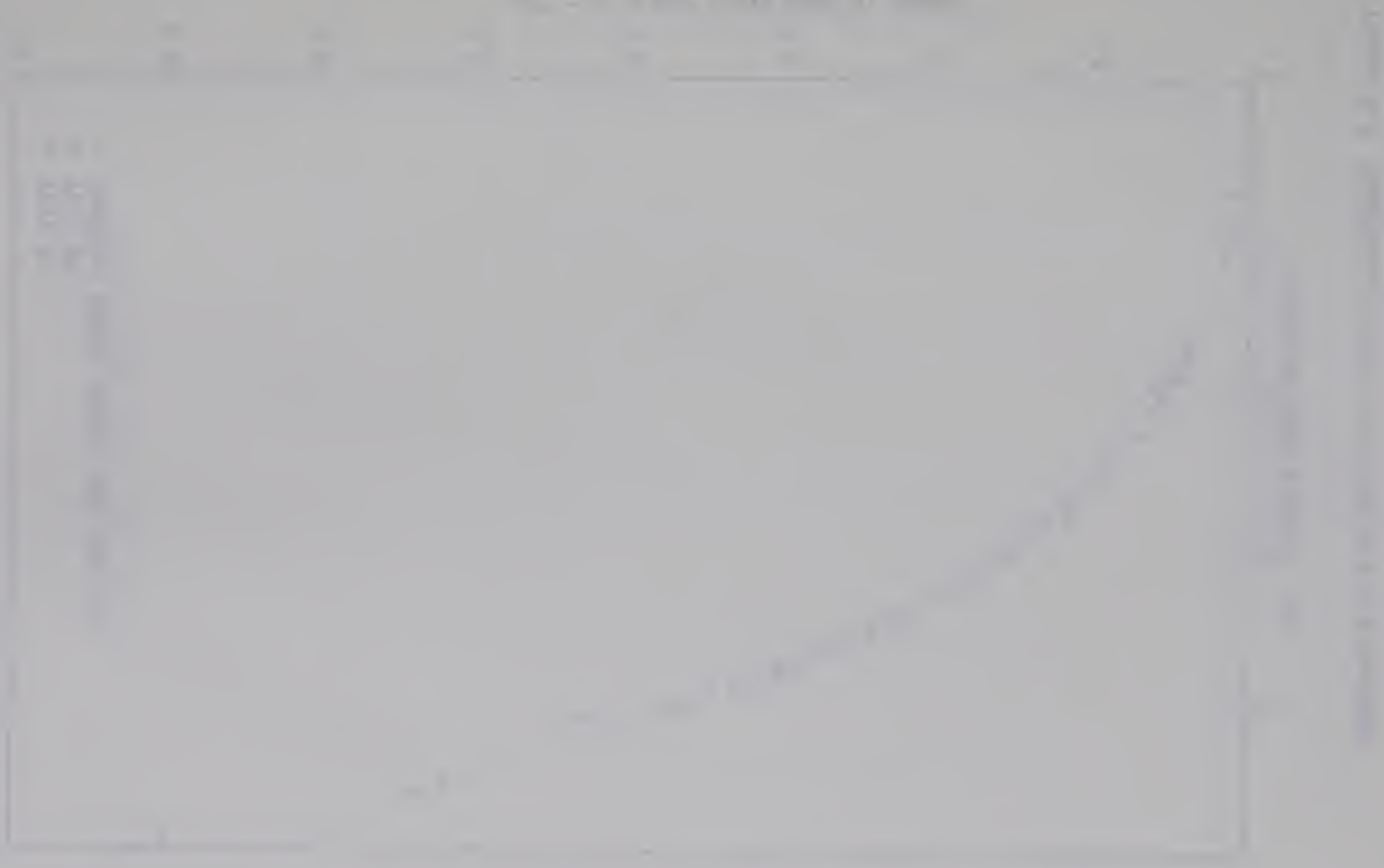

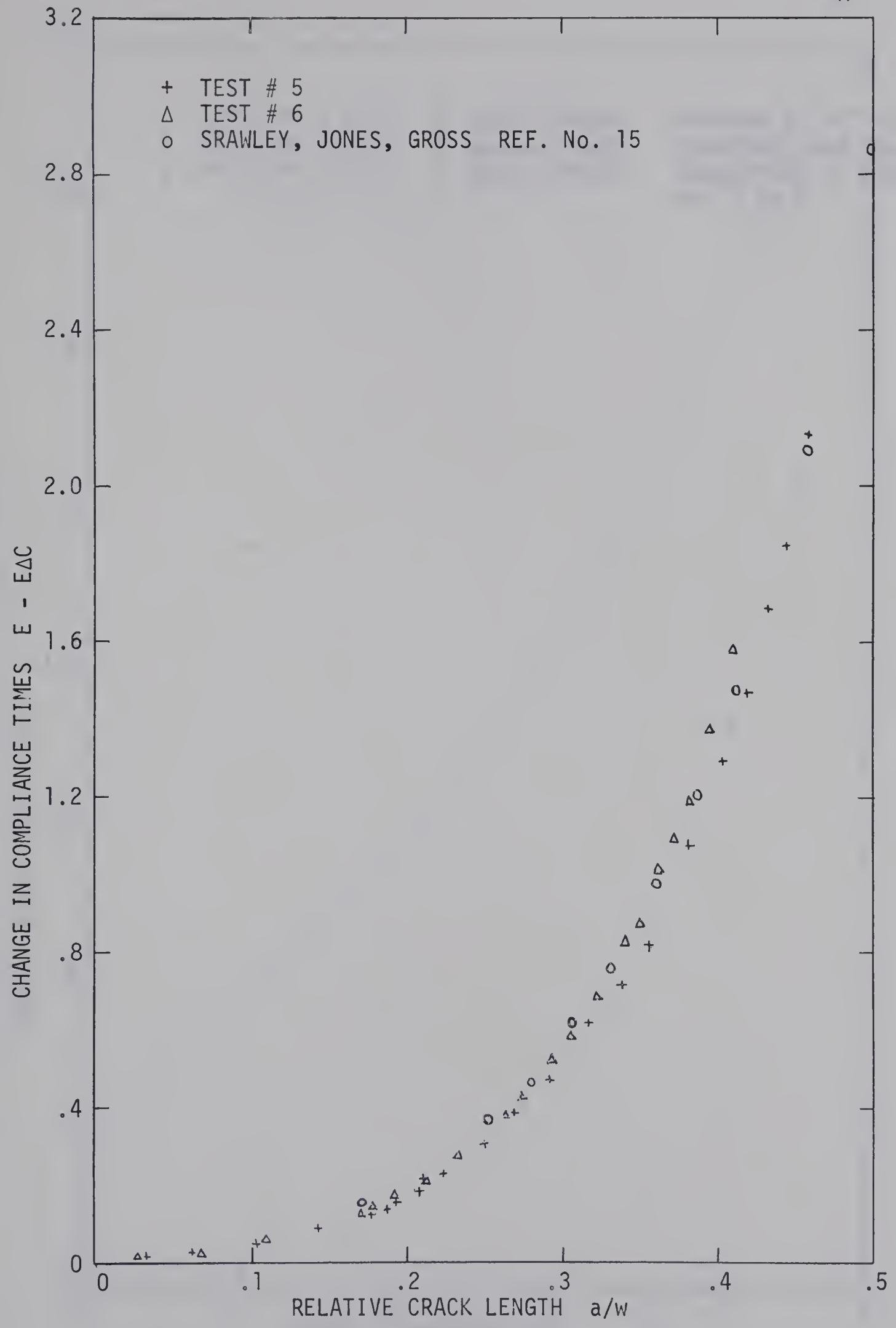

Figure 4.3 Compliance Curves for 0.125 Inch SEN Specimen

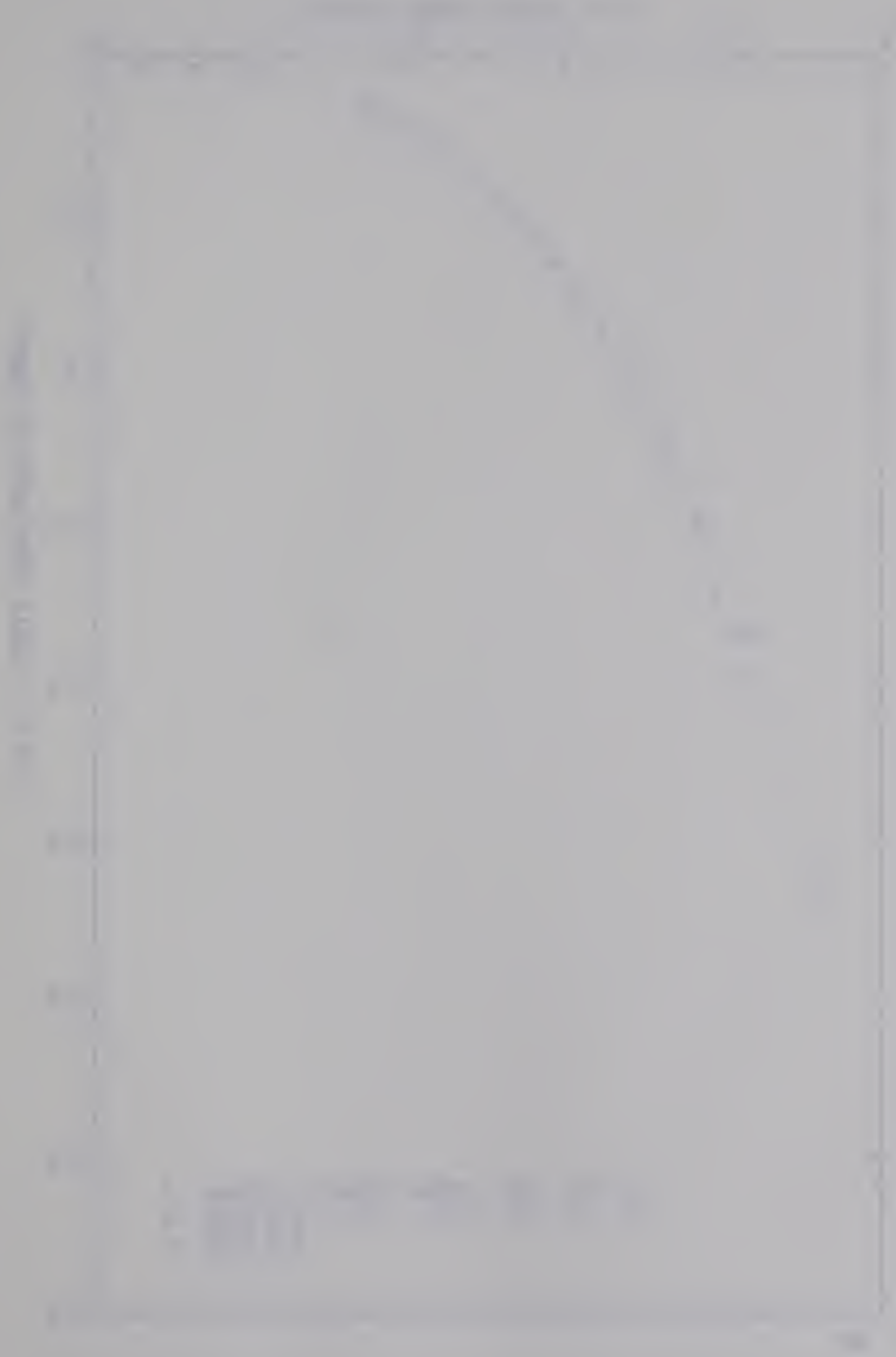

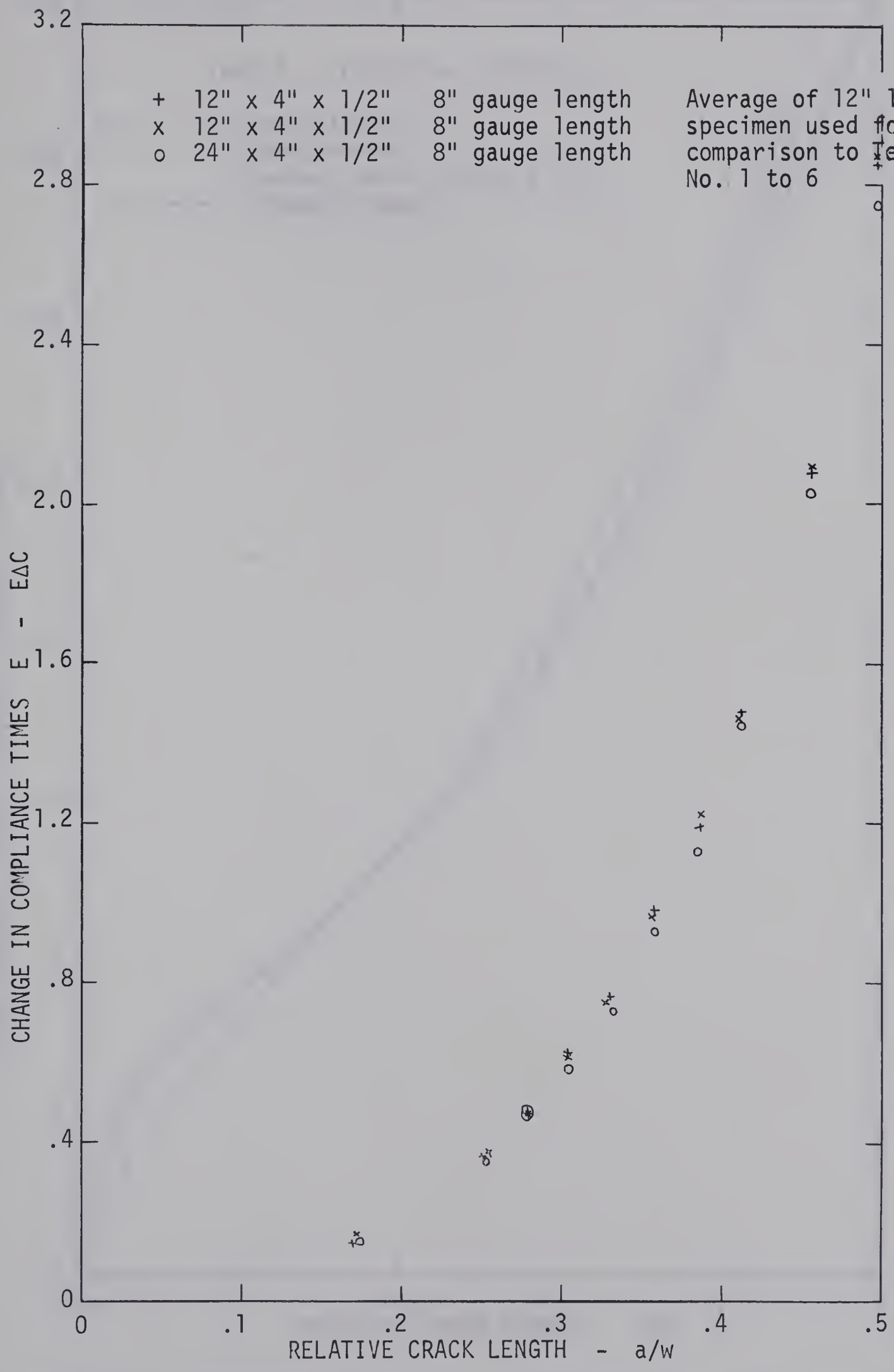

Figure 4.4 Compliance Curves of Srawley, Jones, and Gross [15]

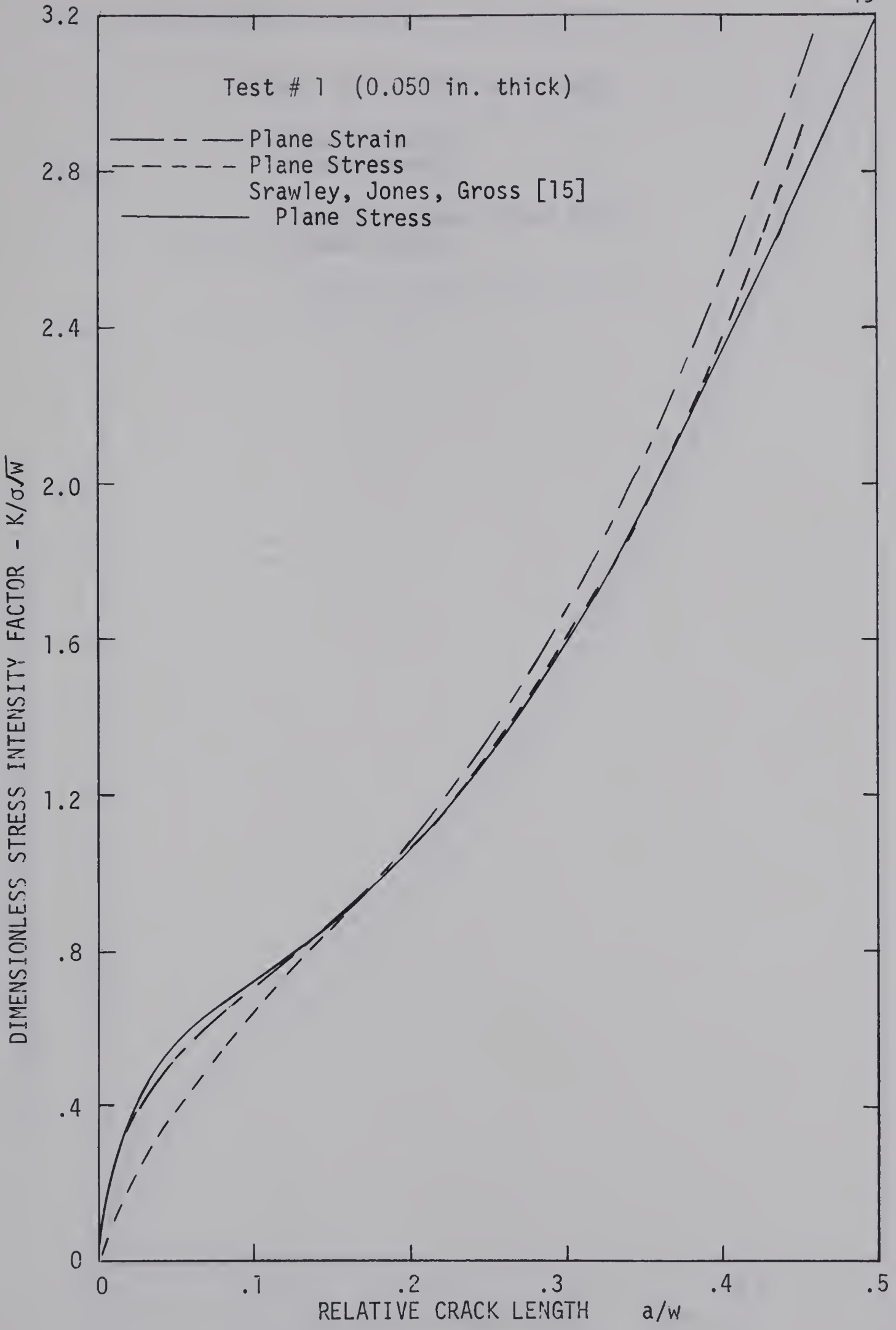

Figure 4.5 Dimensionless Stress Intensity Factor Plot for Test #1

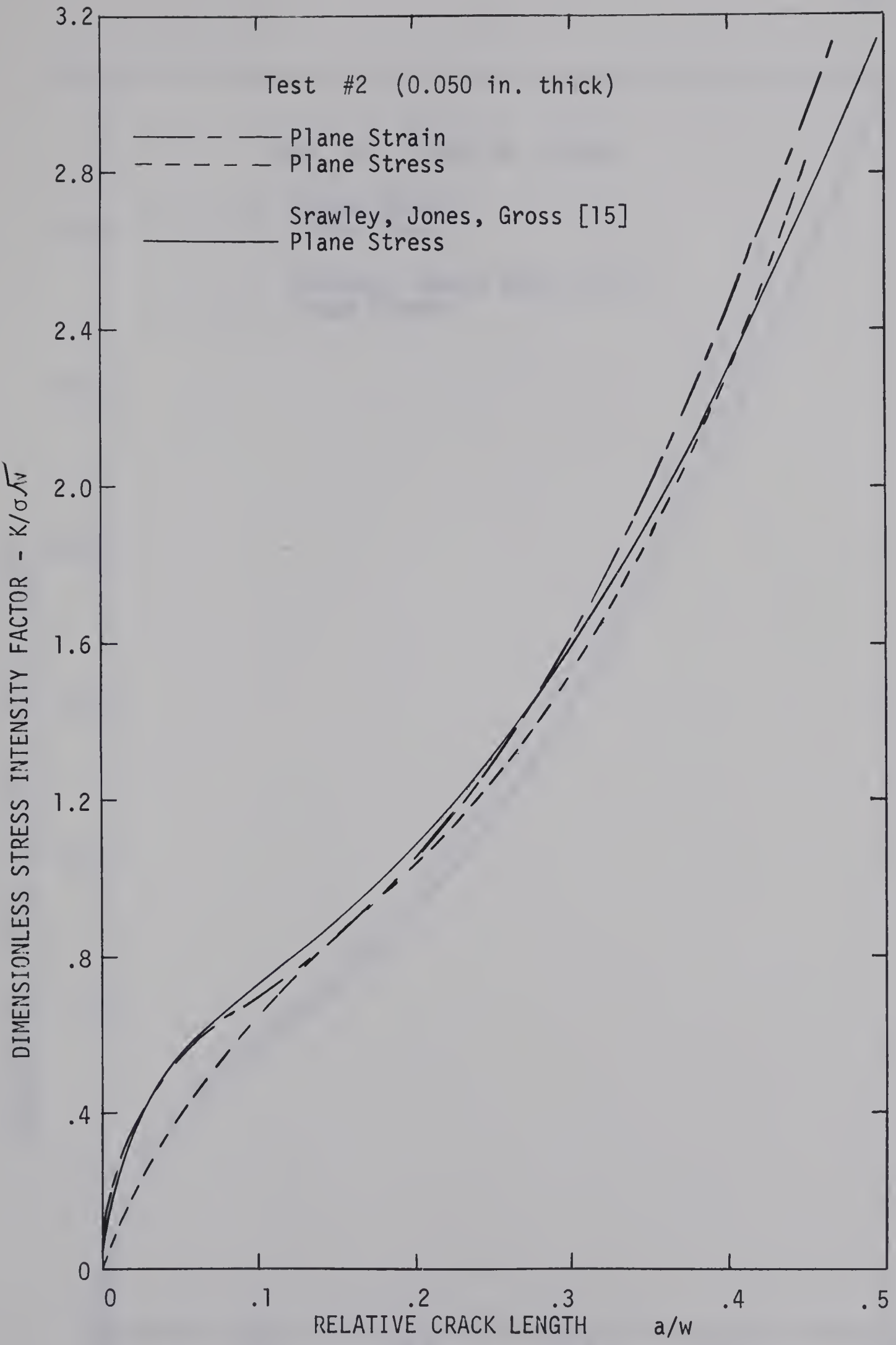

Figure 4.6 Dimensionless Stress Intensity Factor Plot for Test #2

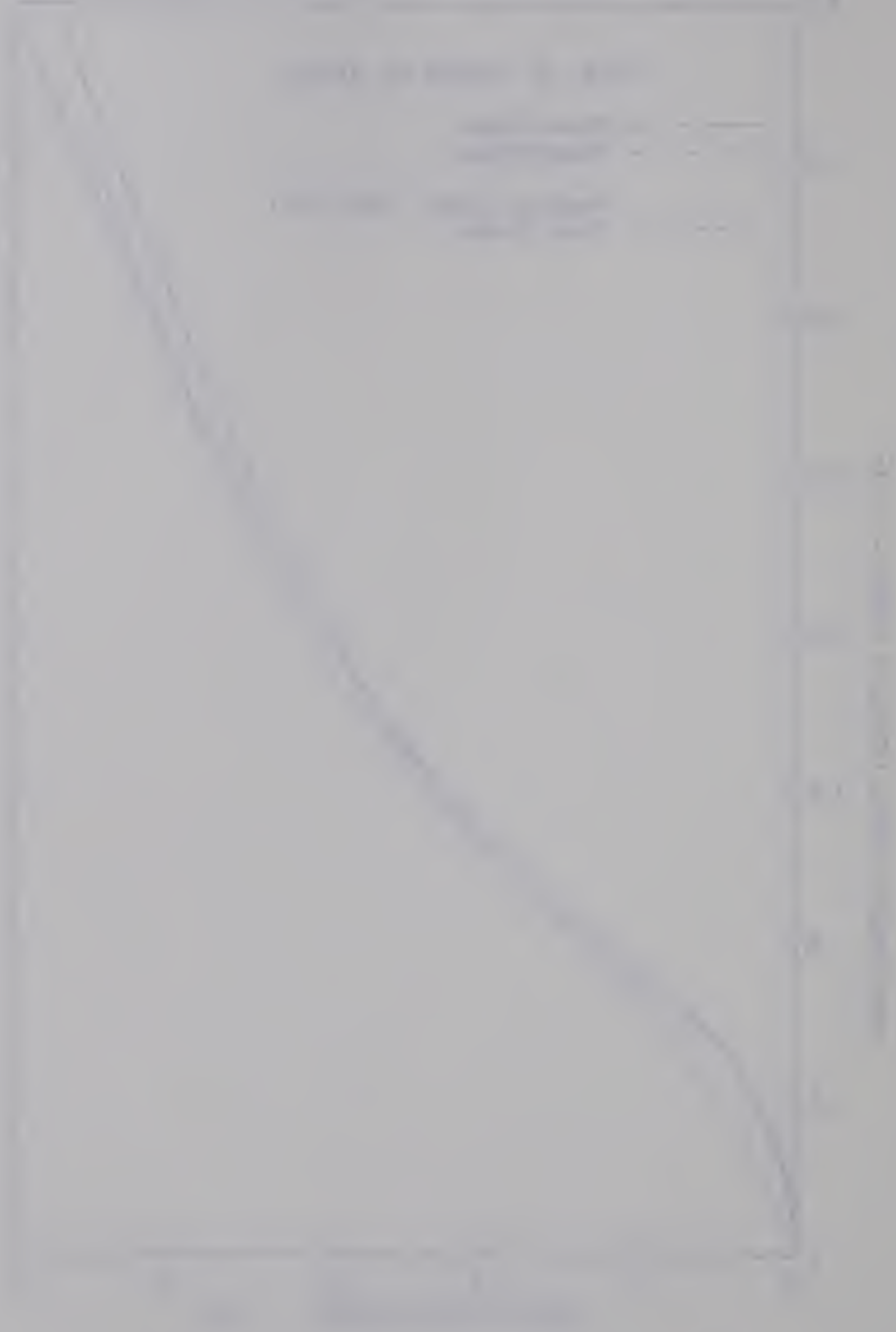

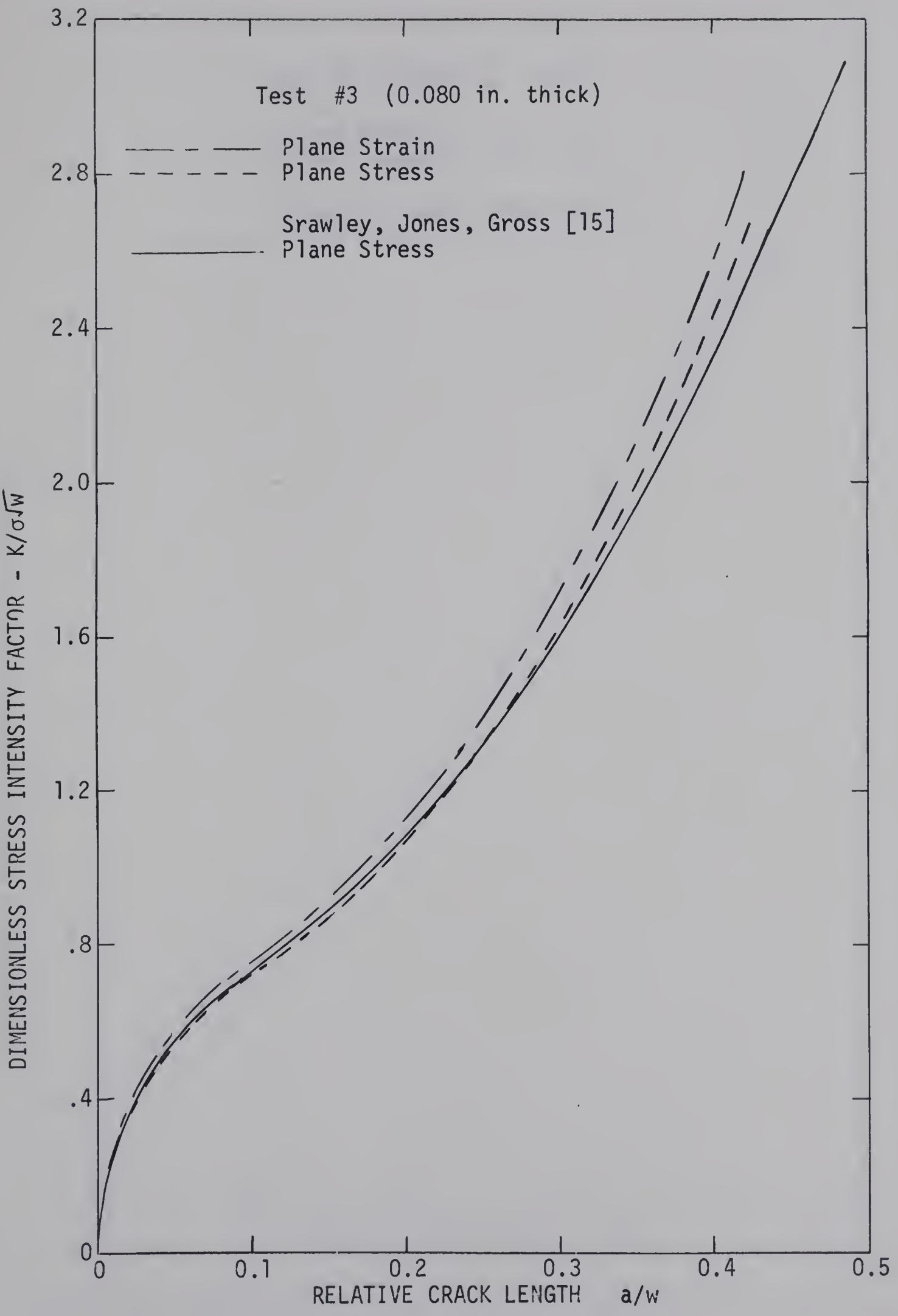

Figure 4.7 Dimensionless Stress Intensity Factor Plot for Test #3

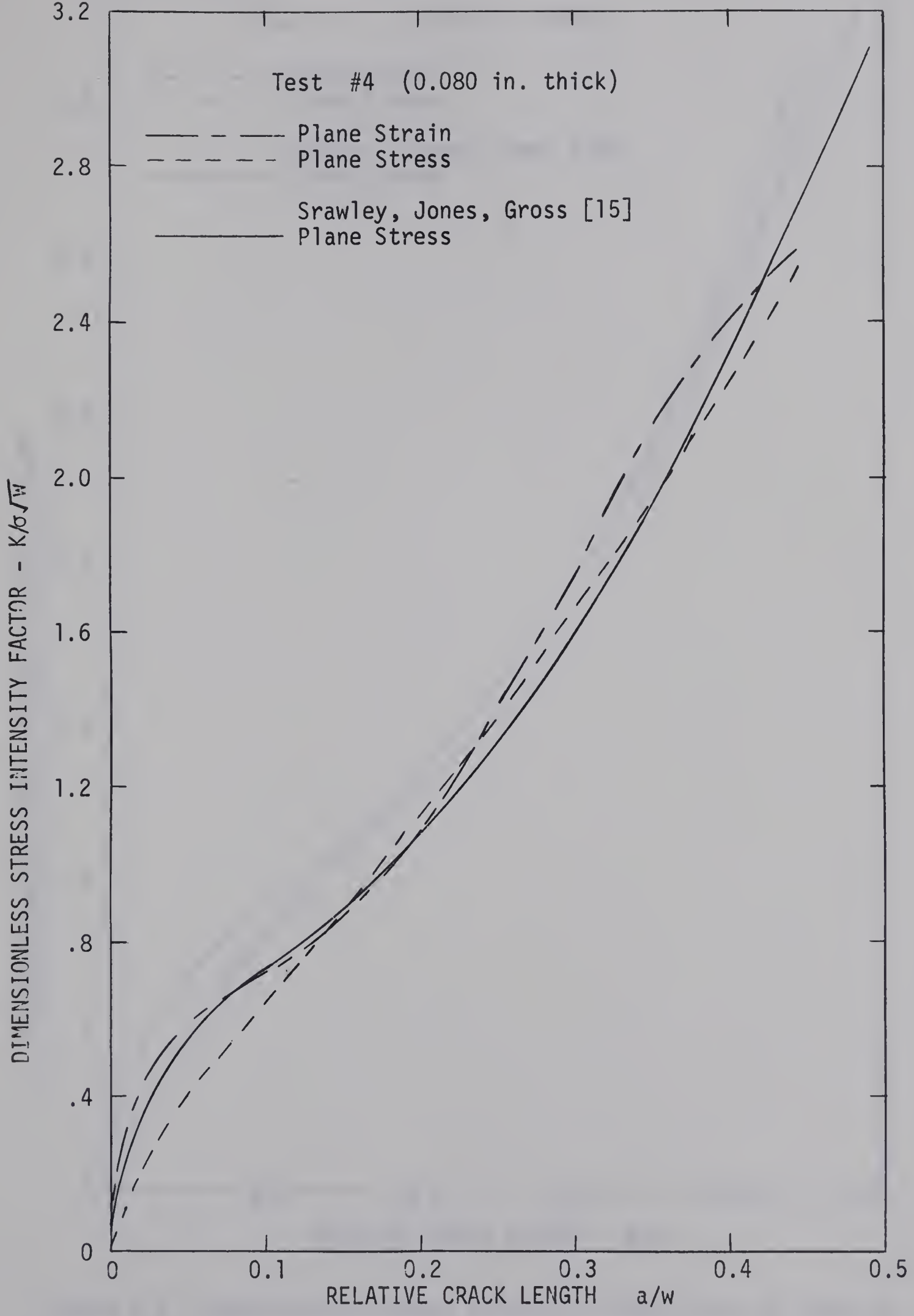

Figure 4.8 Dimensionless Stress Intensity Factor Plot for Test #4

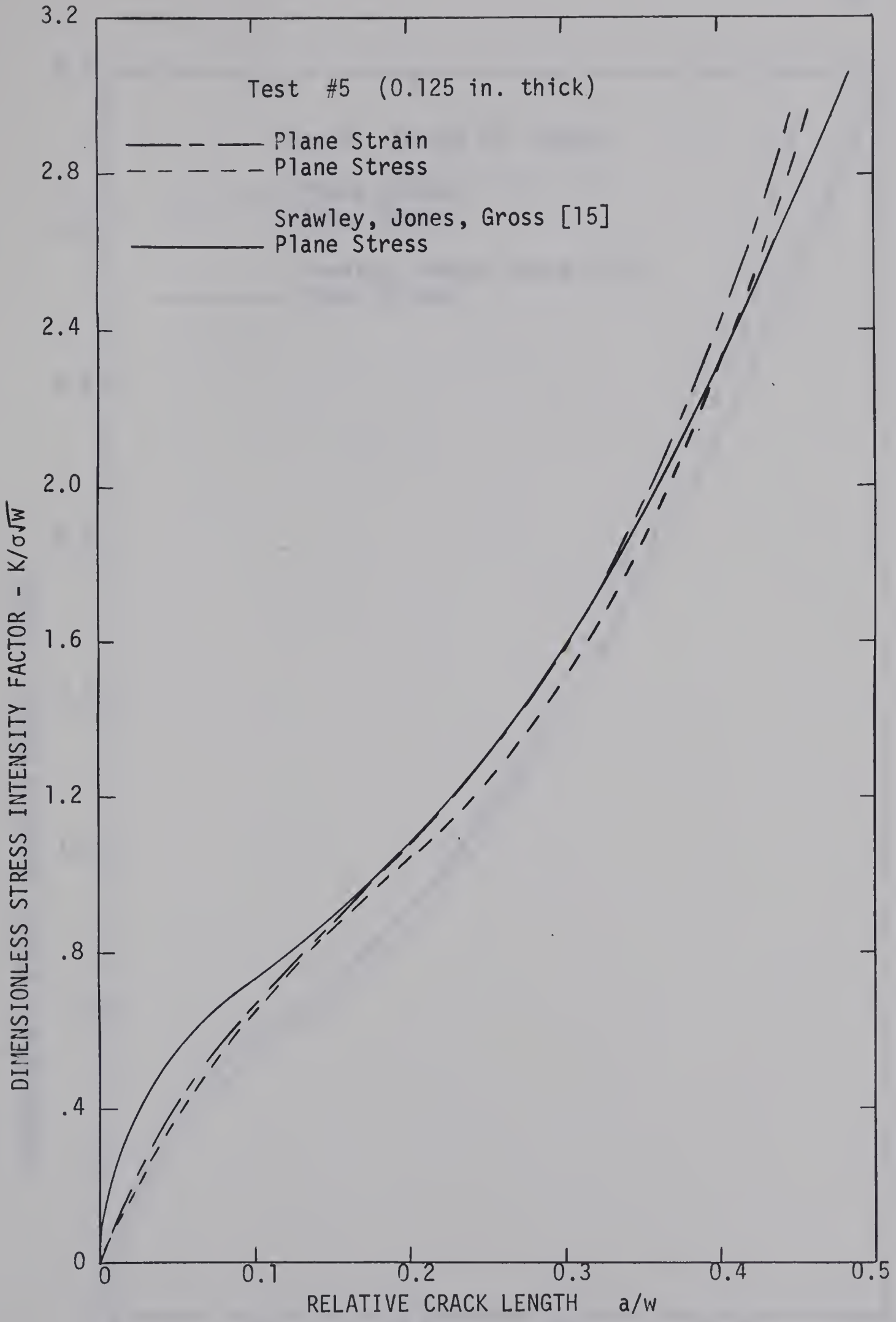

Figure 4.9 Dimensionless Stress Intensity Factor Plot for Test #5

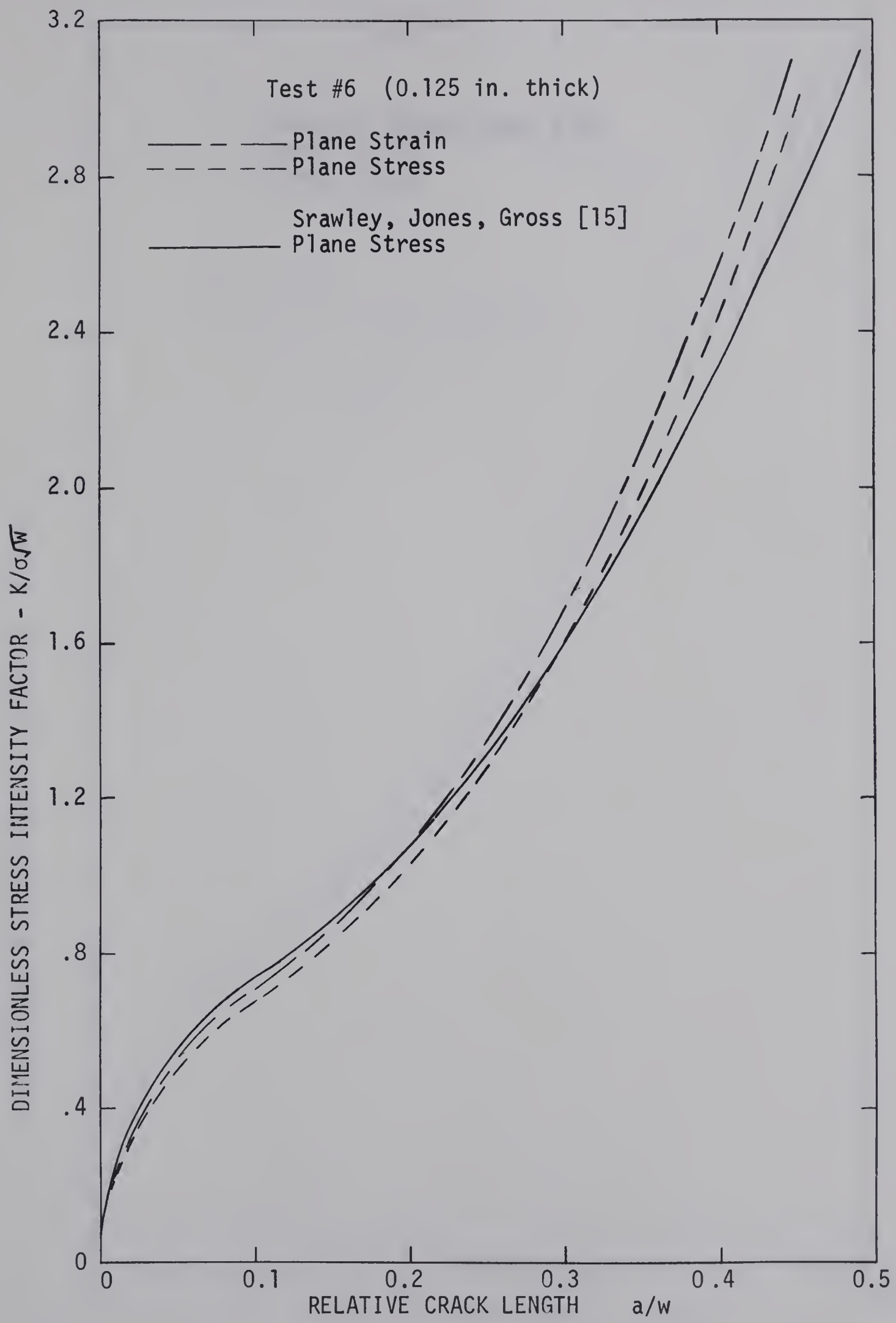

Figure 4.10 Dimensionless Stress Intensity Factor Plot for Test #6

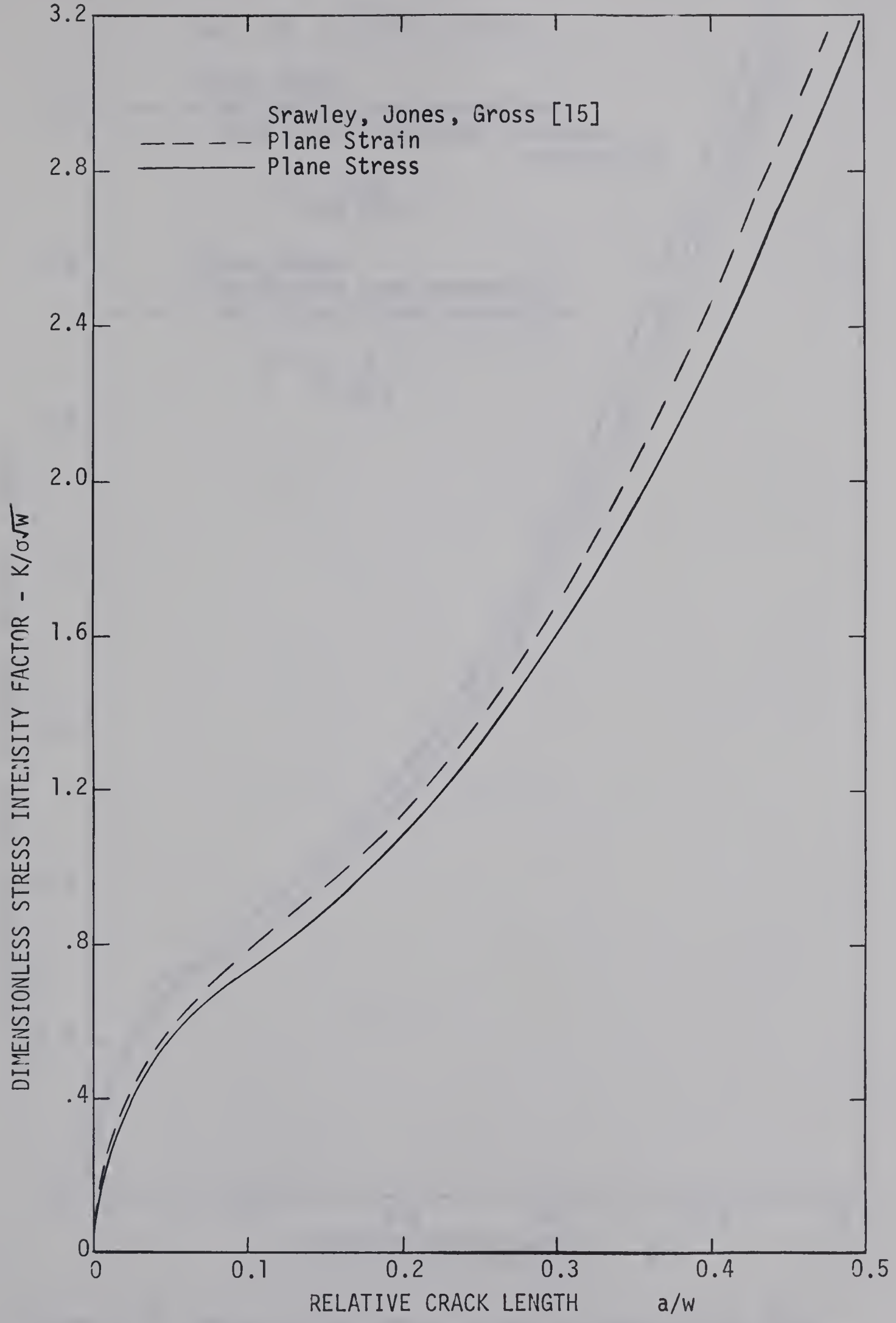

Figure 4.11 Dimensionless Stress Intensity Factor Plot for Srawley, Jones, and Gross [15] 12 Inch Long Specimen

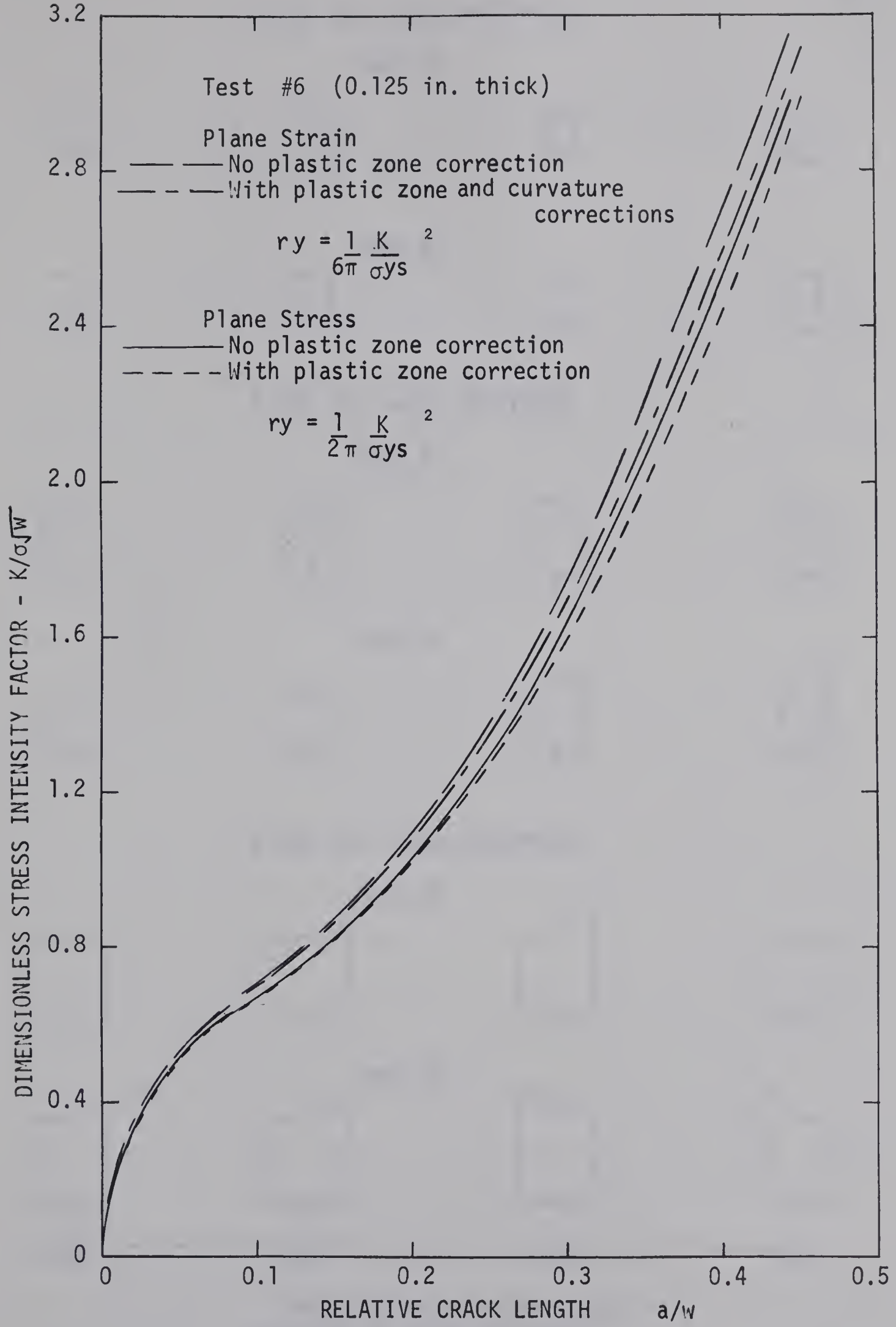

Figure 4.12 Dimensionless Stress Intensity Factor Plots With and Without the Plastic Zone Corrections for Test #6

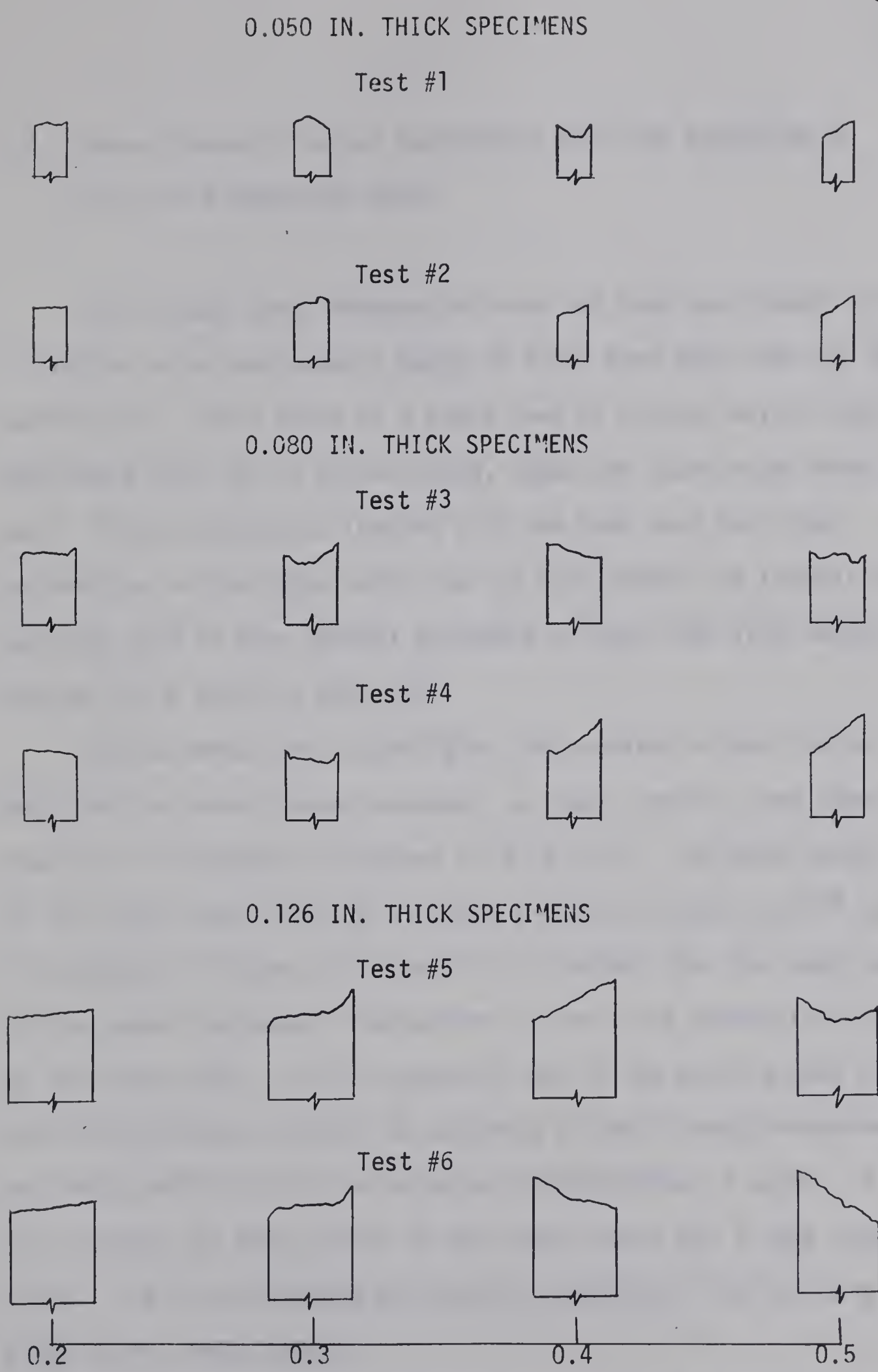

Figure 4.13 Cross-Sections of Crack Surfaces

4.4 Stress Intensity Factor Correlation With the Logarithm of the Crack Propagation Rate.

The fatigue crack propagation rate has been considered to be a function of ΔK and several types of plots have been used for the correlation. Since there is a great deal of scatter using linear coordinate plots of ΔK versus da/dN, logarithm coordinates have been used. The ΔK versus log (da/dN) plot has been used for close observation of test data while the log (ΔK) versus log (da/dN) plot has been used to show general agreement of test data from various sources for a specific material.

The ΔK versus log (da/dN) plot for aluminum alloys can be described as having three branches: a lower, central, and upper branch as illustrated in Figures 4.14 to 4.18. The lower branch of the curve occurs when ΔK is below a value of 6000 $lb(in)^{1/2}$ as illustrated in Figures 4.15 and 4.17. The data for the lower part of the curve indicates a fluctuation in the crack propagation rate as the crack grows. This is possibly due to the crack growth rate being discontinuous and/or the accuracy of crack length measurements not being sufficient for an accurate determination of da/dN. A line through the data points of the lower branch has a very gentle slope. The crack surfaces are usually completely flat for this stage of the crack growth.

The central branch of the curve is indicated in Figures 4.14 to 4.18. A straight line can be drawn through the data points for this branch of the curve. A great deal of scattering can be seen in the curves, and is even more pronounced when the stress ratio R

is of a lower value, as for example in Figure 4.14 and 4.15. The slope and position of the central branch of the curve depends on the specimen thickness. The thinner specimens have slower propagation rate than the thicker specimens for the same value of ΔK as seen from the above figures. Increasing the stress ratio shifts the curve to the right as seen in Figures 4.14 and 4.15 and thus increases the crack propagation rate. The crack surface is in a transition phase changing from flat to slanted over the central branch of the curve.

The upper branch of the correlation is shown in Figure 4.16 and begins at a point where the central portion deviates to the right. The location of this upper portion depends upon the stress ratio. Increasing the stress ratio will cause this portion of the curve to begin at a lower value of ΔK. Thus this portion probably depends more on K than ΔK.

The ΔK versus log (da/dN) plot can be used to illustrate the effects of test variables quite well. In the figures, the effects of specimen thicknesses, stress ratios, and annealing on the crack propagation ratio can be seen.

4.5 Relating the Correlation of the Stress Intensity Factor and Crack Propagation Rate to Electron Fractography

Piper, Quist, and Anderson [25] have plotted data for the aluminum alloy 7178-T6, using the ΔK versus log (da/dN) plot and they discuss the correlation in three branches as in Section 4.4. Electron microfractography studies of the crack surfaces was used

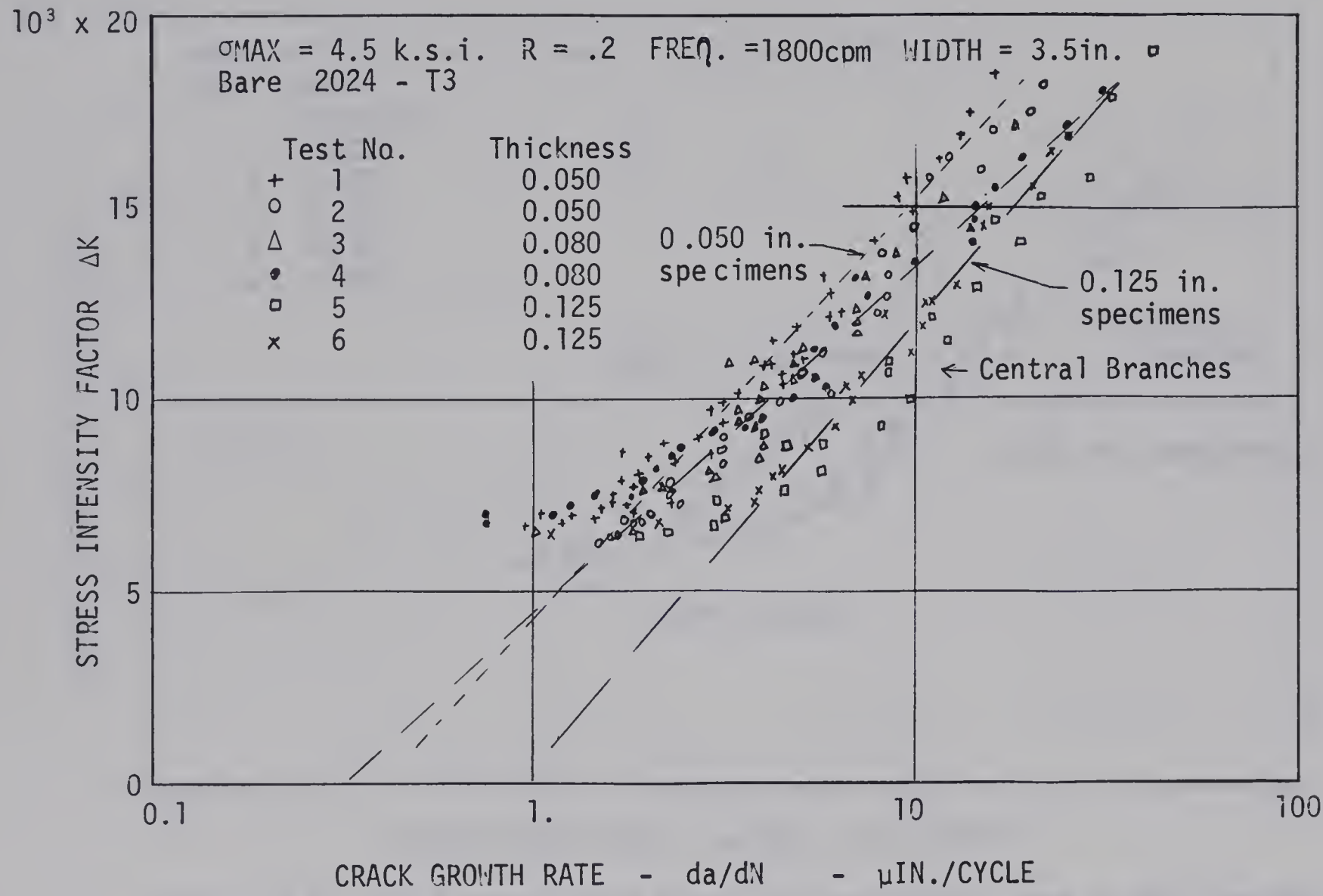

Figure 4.14 Crack Propagation Curve for Test #1 to #6 on SEN Specimen

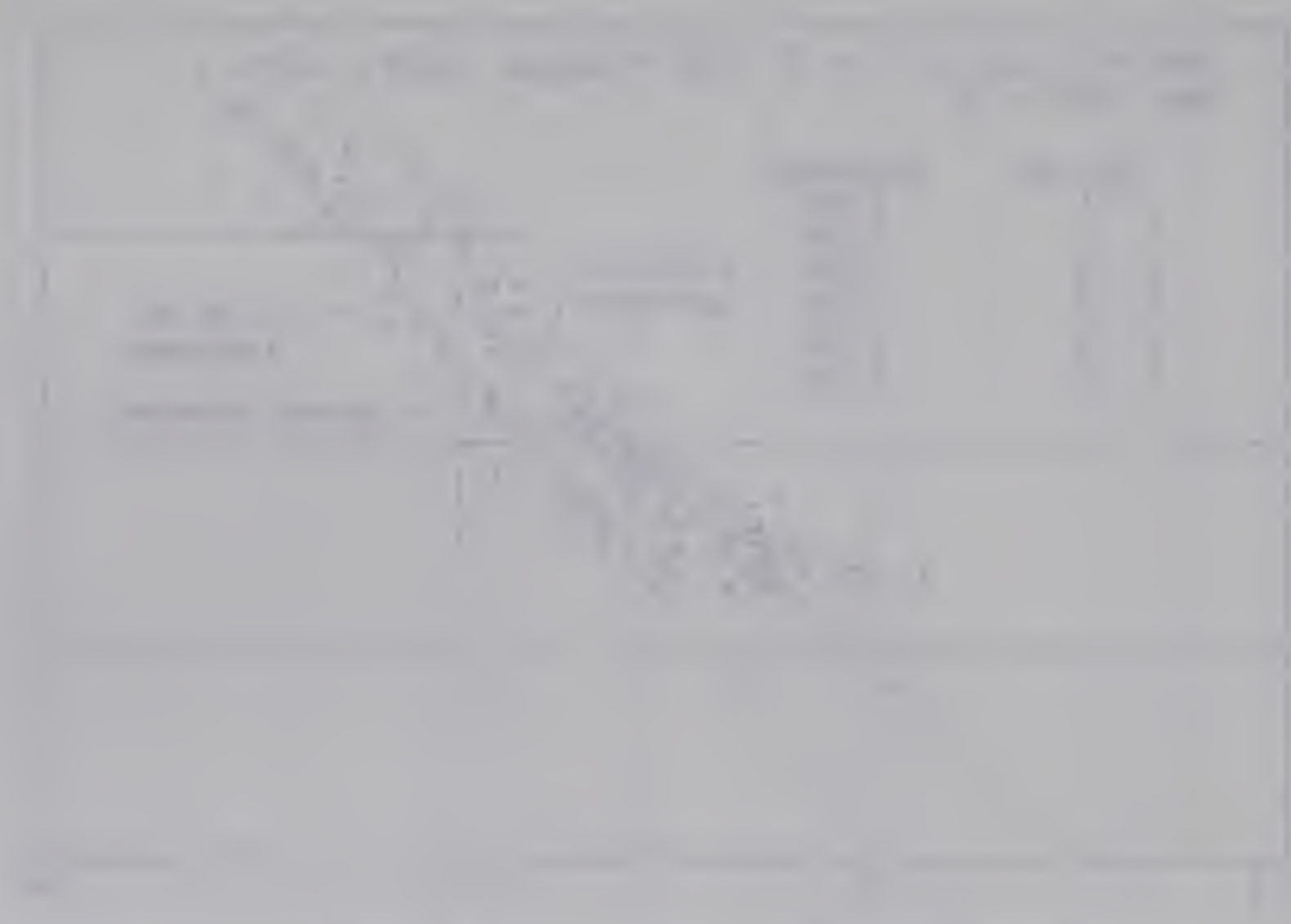

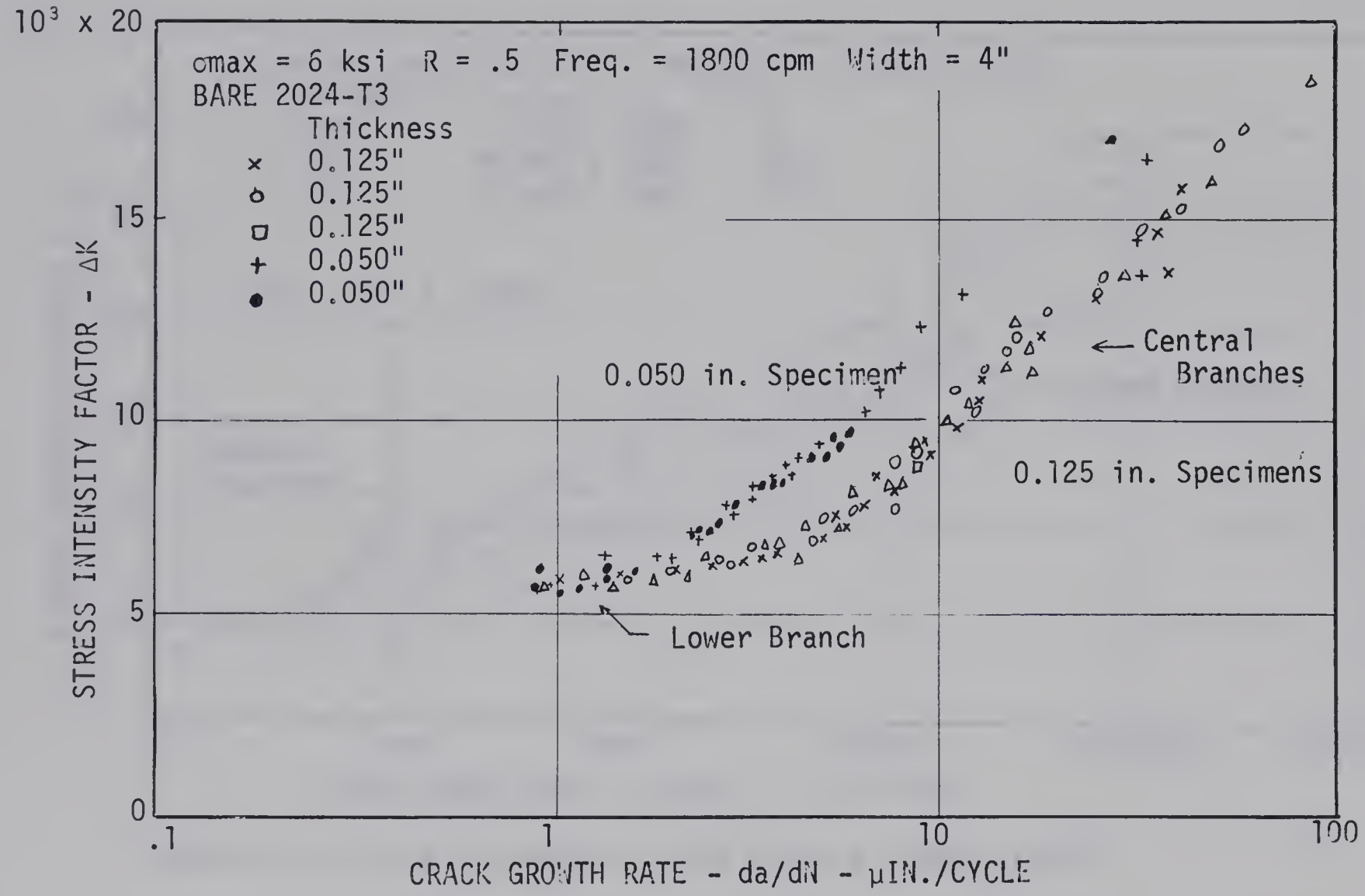

Figure 4.15 Crack Propagation Curve for Preliminary Test on SEN Specimen

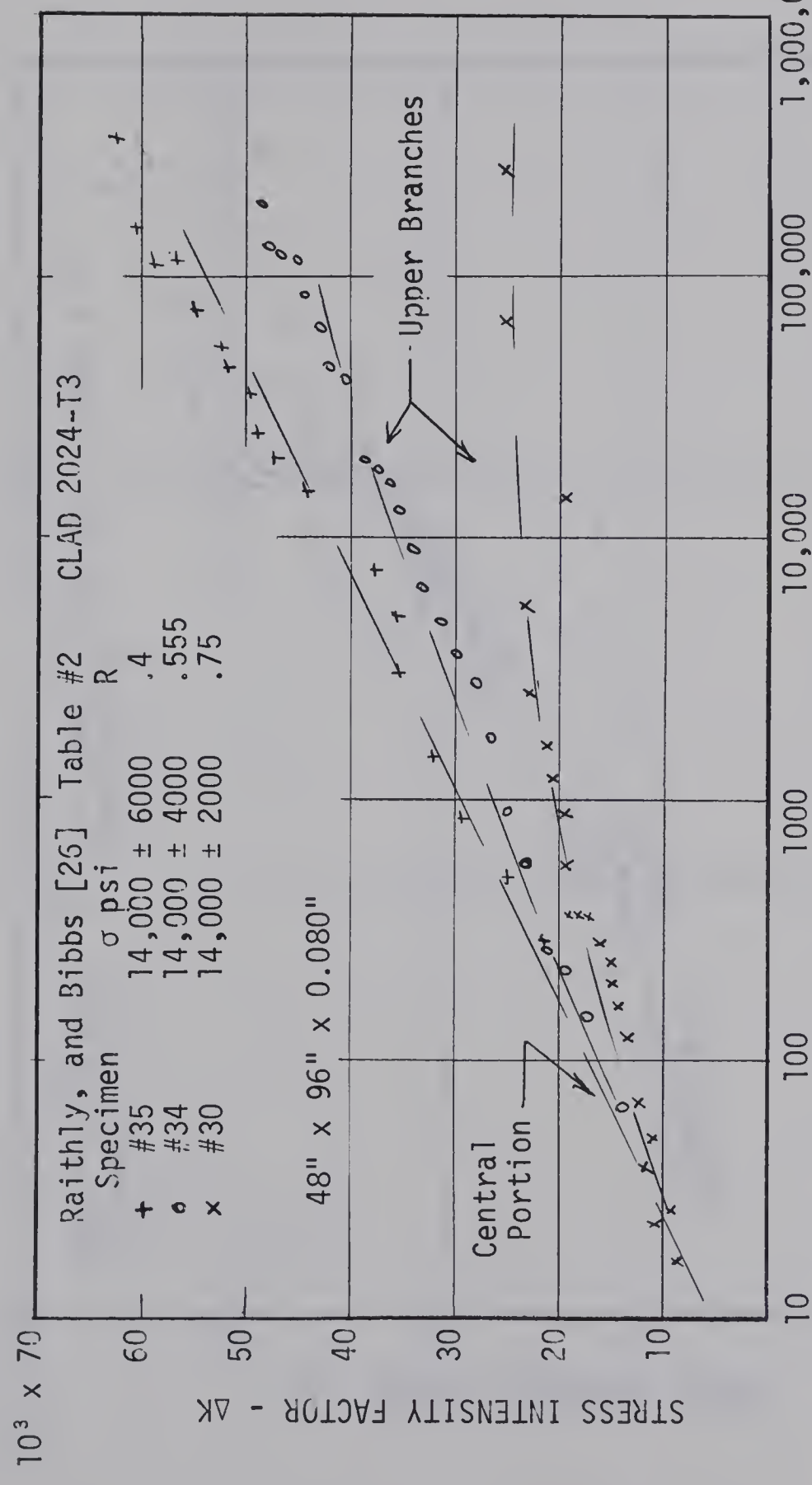

Figure 4.16 Crack Propagation Curve Showing "Upper Branch"

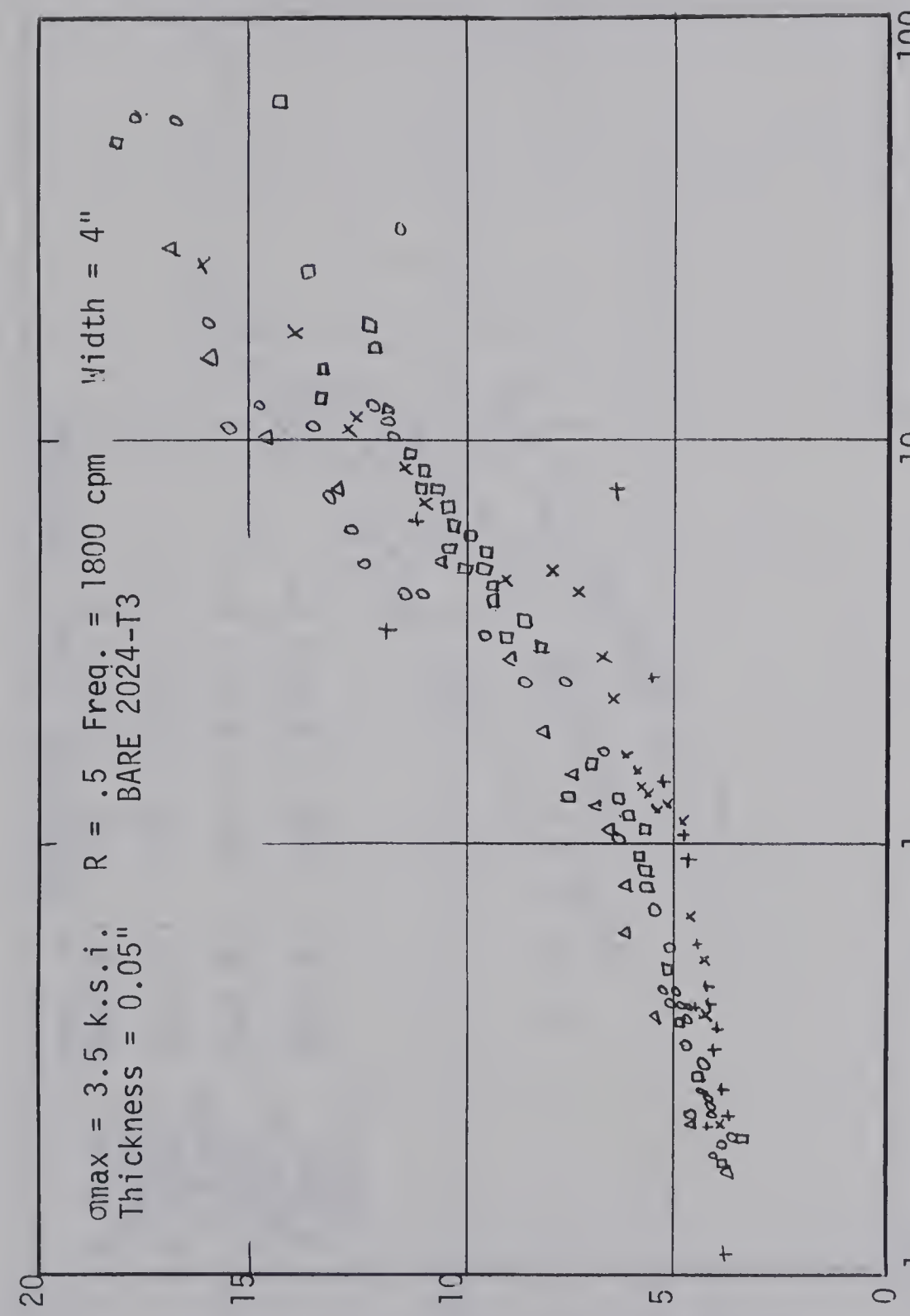

Figure 4.17 Crack Propagation Curve for Preliminary Tests on SEN Specimen

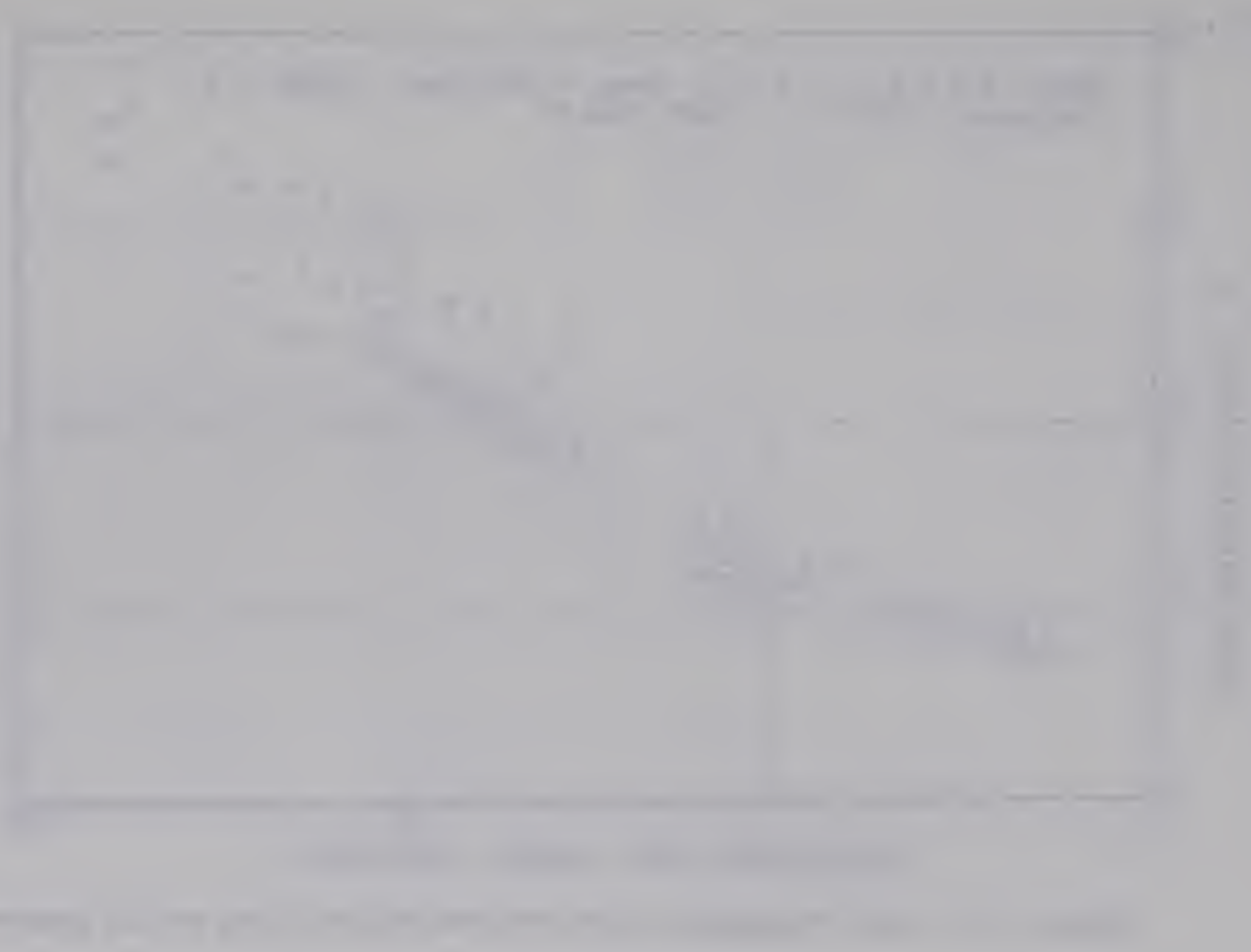

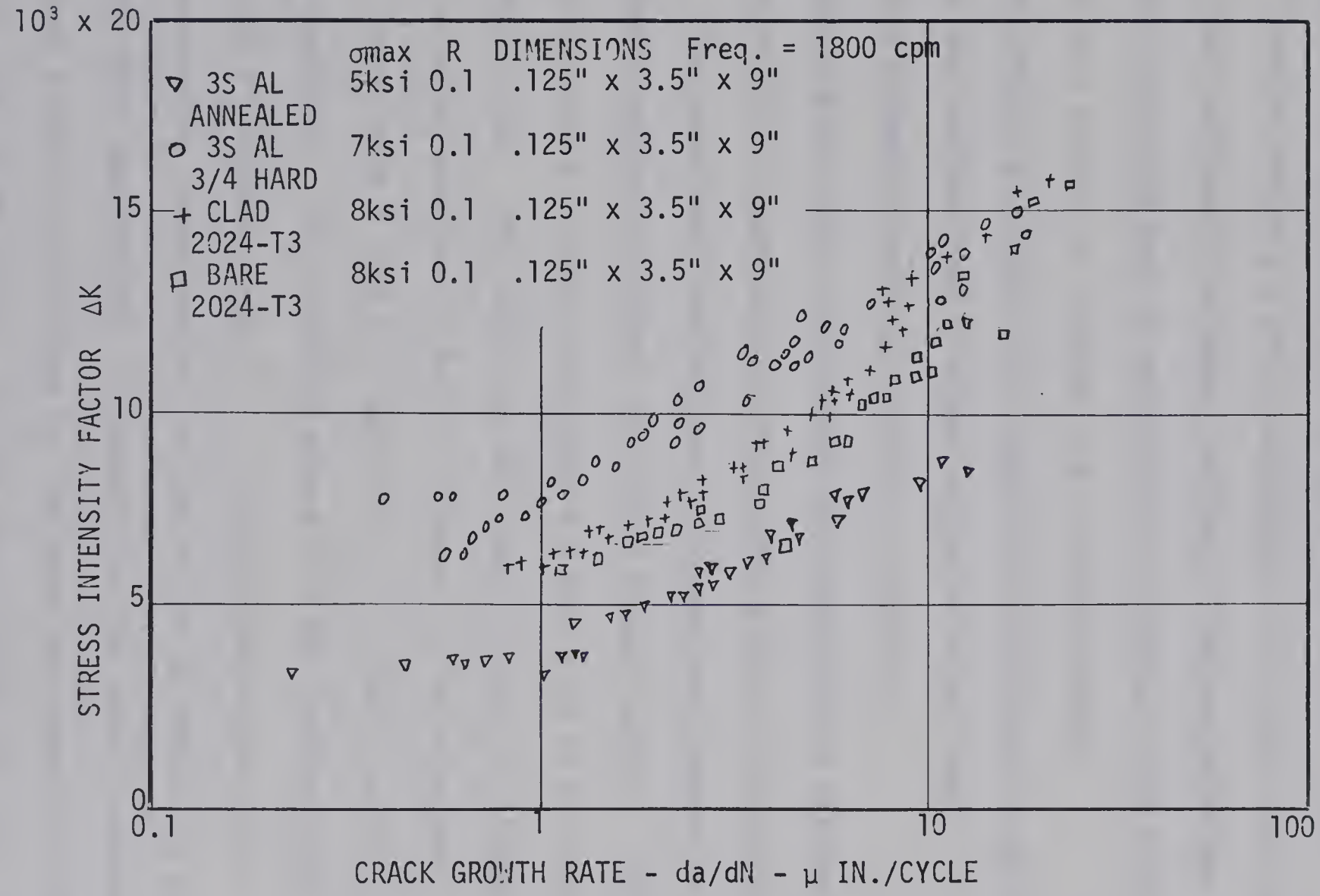

Figure 4.18 Crack Propagation Curve for Preliminary Tests on Center-Notch Specimen

to discuss the "mechanism" of crack growth for each portion of the curve. For the lower portion, fatigue striations were evident over all the replicated area of the crack surface. They were also evident over most of the replicated area of the crack surface of the central portion and only a small percentage of the replicated area of the crack surface of the upper portions. They describe the remaining replicated area as represented by internal voids which coalesce by a process of internal and localized necking.

Christensen and Harmon [12] compare the striations to cyclic loadings and conclude that at higher values of K the crack propagates by means other than producing striations.

Hertzberg and Paris [19] studied the striations on fatigue surfaces of 2024-T3 specimens of thicknesses 0.063, 0.094, and 0.126 inches. They concluded that fatigue striations were present in plane strain regions and absent from plane stress regions. Striations completely covered the flat crack area and only part of the area of the slanted crack. They described the remaining area of slanted cracks as having examples of ductile ruptures called elongated dimples, which have a long axis perpendicular to the direction of crack propagation. The striation agreed with the loading cycles for a crack propagation rate of 1 to 100 microinches per cycle which corresponds to the central portion of the ΔK versus log (da/dN).

From these observations, it appears that the crack propagates in a manner producing striations for the lower and central portions of the ΔK, log (da/dN) curve. For the lower portion the cyclic load probably does not produce striations continuously while in the upper portion of the curve the crack probably propagates by a mechanism

other than that which produces striations. Tetelman and McEvily [10] state that any model used for fatigue crack propagation must account for the striations, and other surface marks, and the observation of plastic deformation taking place at the crack tip.

4.6 Logarithm of Stress Intensity Factor Correlated with Logarithm of Crack Propagation Rate

Paris and Erdogan [18] have used the log (ΔK) versus log (da/dN) plot to show agreement for crack propagation data of 2024-T3 material from various sources. Data for crack propagation rates of less than one micro inch per cycle to 10,000 micro inches per cycle was plotted on the one graph. A straight line of slope 1/4 appeared to fit data for the wide range of crack propagation rates. The equation of the line being

$$\frac{da}{dN} = \frac{(\Delta K)^4}{M} \tag{28}$$

where M is a material constant. Tentatively, equation 28 could be used to predict crack propagation but it basically shows that larger changes in the crack propagation rate may occur for relatively small changes in ΔK.

More recently Roberts and Erdogan [20] have presented a crack propagation equation which accounts for the effect of the stress ratio R as well as ΔK on the crack propagation rates for fluctuating tensile loading and bending loadings. They initially assumed that da/dN should depend on the plastic deformation. Relating the plastic deformation to the stress intensity factors, they found that the

crack propagation rate must be dependent on the stress intensity factors. They assumed the crack propagation equation to be:

$$\frac{da}{dN} = B\left(\frac{1}{1-R}\right)^{\alpha 1} (\Delta K)^{\alpha 2} \tag{29}$$

where B is a material constant. From da/dN tests on 2024-T3 and 7075-T6 materials, they concluded the general da/dN law to be:

$$\frac{da}{dN} = B(K)^2 (\Delta K)^2 \tag{30}$$

or

$$\frac{da}{dN} = B\left(\frac{1}{1-R}\right)^2 (\Delta K)^4 \tag{31}$$

The specific equation that represents the test data of 2024-T3 specimen under fluctuating tension is:

$$\frac{da}{dN} = 2.68 \times 10^{-19} \left(\frac{1}{1-R}\right)^{1.54} (\Delta K)^{3.62} \tag{32}$$

Data of tests 1, 4, and 6 are plotted using log ΔK versus log da/dN coordinate in Figure 4.19 with the equation of each curve shown on the figure. The lines of equations 31 and 32 are shown on the figure for comparison. The test data curves are above the curves of equation 32, but of approximately the same slope. The difference may be due to the higher frequency of the tests or other test parameters that affect da/dN. The data of the 2024-T3 material of Roberts and Erdogan [20] agrees fairly well with that of Hertzberg and Paris [19] but not with the test results of tests 1 to 6. Hertzberg and Paris [19] indicated that higher loading frequencies slowed down the crack propagation rate. Tests numbered 1 to 6 had a loading frequency of 1800 cpm while those of references 19 and 20 were at 140 cpm. The yield stress of the material tested varied between 52 to 57 k.s.i. which was a little higher than the

yield stress of the material used by Hertzberg and Paris [19] (45 k.s.i.). The yield stress was raised to the fourth power and included as part of the material constant in Roberts and Erdogan's work. The difference in the yield stress may be due to differences in properties of the material in manufacturing and/or to age hardening. The age of the 2024-T3 material is unknown and its yield stress might have increased due to the age hardening process.

According to Piper, Quist, and Anderson [25], slight variations of chemical composition may change the mechanical properties more than variations in mill practices. They showed variations of the chemical composition of the 7000 series of aluminum alloys, greatly affected the crack propagation rates and fracture toughness values.

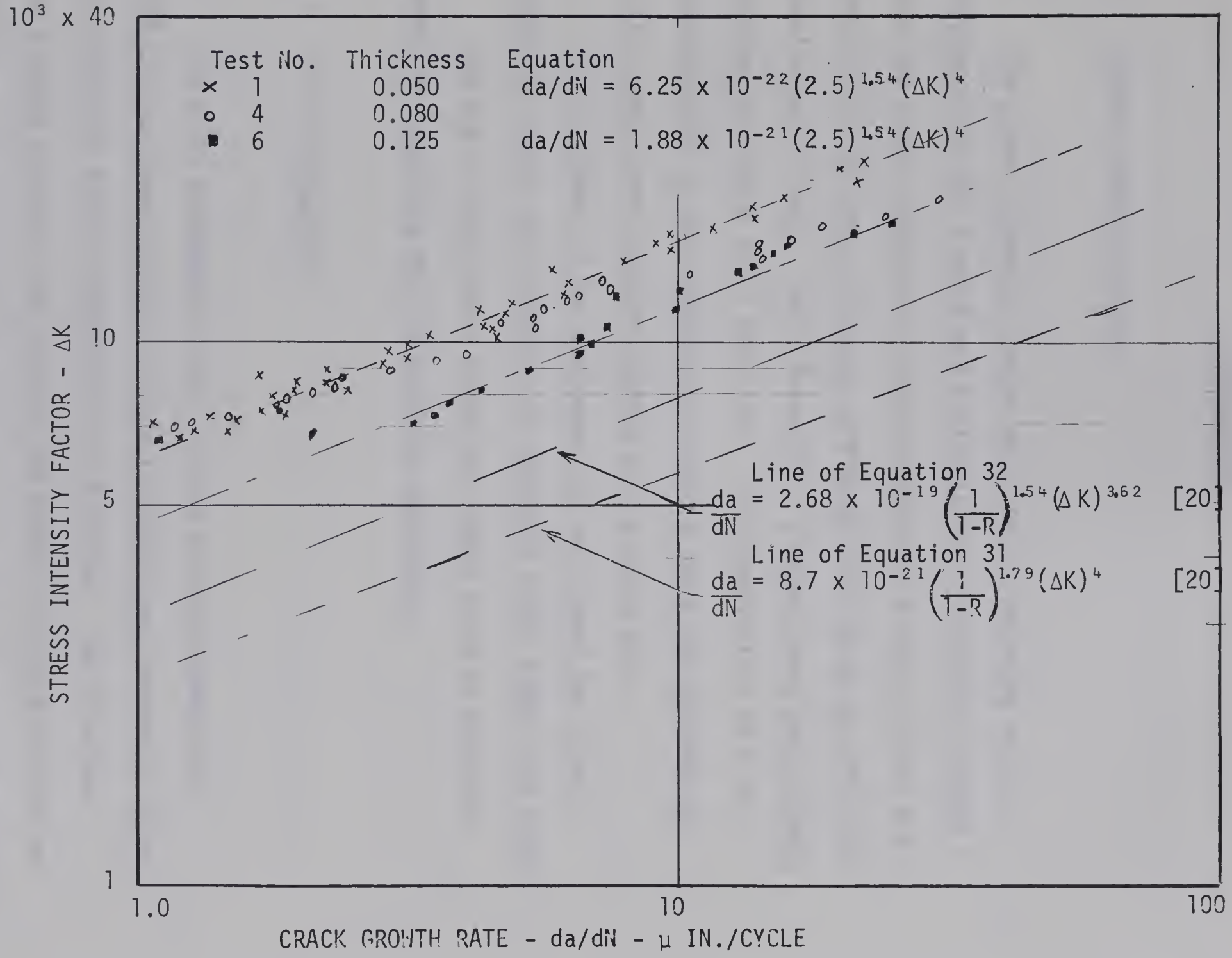

Figure 4.19 Log (ΔK) Versus Log (da/dN)

CHAPTER V

CONCLUSIONS

5.1 Stress Intensity Factor

The stress intensity factor which was found using a flat fatigue crack for a notch and a plastic zone correction, agreed with the stress intensity factors obtained by Srawley, Jones and Gross [15], and Gross, Srawley, and Brown [14] using an artificial ideal elastic crack. The K found for a slanted crack was slightly greater than the K for a flat crack. The application of K to a slanted crack is not completely correct since K was defined for a flat crack under tension loading at the crack tip.

The thickness of the specimens did not affect the stress intensity factor for specimens of thickness 0.05, 0.080, and 0.125.

The use of long strain gauges was found to be an accurate method of measuring the SEN specimen compliance.

5.2 Crack Propagation

The crack propagation rate, for the bare aluminum alloy 2024-T3, was found to be a function of the stress intensity factor, ΔK, with many factors affecting this function. The ΔK versus log (da/dN) plot was used to show the effect of single factors on the da/dN, ΔK function. The lower part of the plot was unaffected by specimen thickness whereas for the other parts of the plot, the thinner specimens (0.050 inches) had a slower crack propagation

rate than the thicker specimens (0.125 inches) for the same value of ΔK. The log ΔK versus log da/dN plot was found useful in showing agreement of a wide range of data for one material and for comparison of crack propagation properties of various materials.

Increasing the stress range caused increases in the crack propagation rate for a given value of ΔK. Roberts and Erdogan [20] incorporated the effects of R in the crack propagation equation. The crack propagation rate was written as a function of R and ΔK. From tests, the exponent of the ΔK term in the da/dN equation was found to be 4 and agreed with that of Roberts and Erdogan [20] and Hertzberg and Paris [18].

The 2024-T3 aluminum alloy used in tests had a slower crack propagation rate than that of references 20 and 18, which caused a significant difference of the material constants in crack propagation equation. Reasons for the slower crack propagation rate might be attributed to the higher frequency of the cyclic loading (1800 cpm as compared to 140 cpm) and to the higher yield strength (56,000 psi as compared to 45,000 psi).

The transition of a fatigue crack surface from being flat to slanted appears to depend on the plastic zone size and is an indication of a change from plane strain condition to a plane stress condition. The transition for thinner specimens (0.050 inches) was more irregular than that of thicker specimens (0.125 inches) and occurred over a shorter period of crack growth.

The stroboscope and high power microscope were successfully used to enable continuous measurement of the crack length during testing.

BIBLIOGRAPHY

1. Gohn, G.R., "Fatigue of Metals, Part 1 - The Mechanism of Fatigue," Material Research and Standards, Vol. 3, 1963, p. 106 - 115.
2. Hardrath, H.F., "Fatigue of Metals, Part 2 - Crack Propagation and Final Failure," Material Research and Standards, Vol. 3, 1963, p. 116 - 121.
3. Griffith, A.A., "The Phenomena of Rupture and Flow in Solids," Philosophical Transaction of Royal Soc. (London), Series A, Vol. 221, 1920, p. 163 - 198.
4. Weiss, V. and Yukawa, S., "Critical Appraisal of Fracture Mechanics," Fracture Toughness Testing and Its Applications, ASTM STP 381, 1964, p. 1 - 29.
5. Irwin, G.R. and Kies, J.A., "Critical Energy Rate Analysis of Fracture Strength," Welding Journal Res Supplement, Vol. 33, 1954, p. 1935 - 1985.
6. Irwin, G.R., "Analysis of Stresses and Strains Near the End of a Crack Traversing a Plate," Journal of Applied Mechanics, Vol. 24, 1957, p. 361.
7. Peterson, R.E., "Fatigue of Metals Part 3 - Engineering and Design Aspects," Material Research and Standards, Vol. 3, 1963, p. 122 - 139.
8. Mowbray, A.O., "Assault on Fracture Pays Off," Material Research and Standards, Vol. 4, 1964, p. 103.

9. International Congress on Fracture, Proceeding of the First International Conference on Fracture, Vol. 1, 2, and 3, 1966.

10. Telelman, A.S. and McEvily, A.J., Fracture of Structural Materials, 1967.

11. Sullivan, A.M., "New Specimen Design for Plane-Strain Fracture Toughness Tests," Material Research and Standards, Vol. 4, No. 1, Jan. 1964, p. 20 - 24.

12. Christensen, R.H. and Harmon, M.B., "Limitations of Fatigue-Crack Research in the Design of Flight Vehicle Structures," Douglas Paper No. 3776, June 1966.

13. Gross, B., Srawley, J.E. and Brown, W.F. Jr., "Stress Intensity Factors for a Single-Edge-Notch Tension Specimen by Boundary Collocation of a Stress Function," NASA TN D-2395, 1964.

14. Paris, P.E. and Sih, G.C., "Stress Analysis of Cracks," Fracture Toughness Testing and Its Applications, ASTM STP No. 381, 1964, p. 30 - 81.

15. Srawley, J.E., Jones, M.H., and Gross, G., "Experimental Determination of the Dependence of Crack Extension Force on Crack Length for a Single-Edge-Notch Tension Specimen," NASA TN D-2396, 1964.

16. Westergaard, H.M., "Bearing Pressures and Cracks," Trans ASME, Journal of Applied Mechanics, Vol. 61, 1939, p. A-49 - A-50.

17. Irwin, G.R., "Crack Toughness Testing of Rate Sensitive Materials," Trans ASME, Journal of Engineering Power, Vol. 86, October 1964, p. 444 - 450.

18. Paris, P.C. and Erdogan, F., "A Critical Analysis of Crack Propagation Laws," Trans ASME, Journal of Basic Eng., 1963, p. 528 - 534.

19. Hertzberg, R.W. and Paris, P.C., "Applications of Electron Fractography and Fracture Mechanics," Proceeding of the First International Conference on Fracture, Vol. 1, p. 459 - 478.

20. Roberts, R. and Erdogan, F., "The Effect of Mean Stress on Fatigue Crack Propagation in Plates Under Extension and Binding," ASTM Paper No. 67-WA/Met-2, 1967.

21. Irwin, G.R., "Fracture Mode Transition for a Crack Traversing a Plate," ASTM Trans, Journal of Basic Eng., Vol. 82, June 1960, p. 417 - 420.

22. Lapidus, L., Digital Computations for Chemical Engineers, McGraw-Hill, 1962, p. 329.

23. ASTM Special Committee, "Fracture Testing of High Strength Sheet Materials," Part. I, ASTM Bull. 243, Jan. 1960, p. 29 - 40; Part II, ASTM Bull. 244, Feb. 1960, p. 18 - 28.

24. Srawley, J.E. and Brown, W.F. Jr., "Fracture Toughness Testing Methods," Fracture Toughness Testing and Its Applications, ASTM STP No. 381, 1964, p. 133 - 198.

25. Piper, D.E., Quist, W.E., and Anderson, W.E., "The Effect of Composition on the Fracture Properties of 7178-T6 Aluminum Alloy Sheet," Application of Fracture Toughness Parameters to Structural Metals, Met. Soc. Conference, Vol. 31, 1966, p. 250 - 269.

26. Raithby, K.D. and Bibbs, M.E., "Propagation of Fatigue Cracks in Wide Unstiffened Aluminum Alloy Sheets," Ministry of Aviation, Aeronautical Research Council, Paper C.P. No. 655, Sept. 1961.